Arctic Science

OPEN ACCESS | Review

Science highlights from the Kjell Henriksen Observatory on Svalbard

Katie Herlingshaw[a], **Noora Partamies**[a], **Charlotte M. van Hazendonk**[a,b], **Mikko Syrjäsuo**[a], **Lisa J. Baddeley**[a], **Magnar G. Johnsen**[c], **Nina K. Eriksen**[a,b], **Ian McWhirter**[d], **Anasuya Aruliah**[d], **Mark J. Engebretson**[e], **Kjellmar Oksavik**[a,b], **Fred Sigernes**[a], **Dag A. Lorentzen**[a], **Takanori Nishiyama**[f], **Matthew B. Cooper**[g], **John Meriwether**[g], **Stein Haaland**[a], **and Daniel Whiter**[h]

[a]Department of Geophysics, The University Centre in Svalbard, Longyearbyen, Norway; [b]Department of Physics and Technology, University of Bergen, Bergen, Norway; [c]Tromsø Geophysical Observatory, UiT, The Arctic University of Norway, Tromsø, Norway; [d]Atmospheric Physics Laboratory, University College London, London WC1E 6BT, UK; [e]Department of Physics, Augsburg University, Minneapolis, MN, USA; [f]National Institute of Polar Research, 10-3, Midoricho, Tachikawa, Tokyo 190-8518, Japan; [g]Center for Solar-Terrestrial Research, New Jersey Institute of Technology, Newark, NJ, USA; [h]School of Physics & Astronomy, University of Southampton, Southampton, UK

Corresponding author: **Katie Herlingshaw** (email: katieh@unis.no)

Abstract

The Kjell Henriksen Observatory (KHO) is the world's largest optical observatory for auroral and airglow measurements, operated by the University Centre in Svalbard (UNIS). KHO is a unique site that lies underneath the dayside cusp, a funnel-shaped region where particles from the Sun can directly enter the Earth's upper atmosphere, including the ionosphere. Building on the pioneering observations of its predecessor—the Auroral Station in Adventdalen, Svalbard—KHO has played a pivotal role in advancing our understanding of phenomena in the polar atmosphere. The Auroral Station and KHO have amassed climatological measurements over Svalbard for an impressive 40-year period. KHO's diverse instrumentation, combined with other co-located optical and radar infrastructure, and in situ measurements from satellites and sounding rockets, has paved the way for impactful multi-instrument studies. Serving as an accessible testbed for instrument development, new types of instruments have recently been installed, both at KHO and on satellites. Beyond its scientific contributions, KHO has become an integral part of the Longyearbyen community, with students, visitors, and locals participating in tours and educational initiatives. This connection underscores KHO's multi-functional role, not only as a centre for excellent research but also as a vital hub for public outreach and engagement.

Key words: Svalbard, space physics, Aurora, ionosphere, Kjell Henriksen Observatory

1. Introduction

The Kjell Henriksen Observatory (KHO) is the world's northernmost auroral observatory. It is located on the archipelago of Svalbard, 800 km north of mainland Norway. The observatory is positioned on the Breinosa mountain, approximately 15 km from the town of Longyearbyen. The geographic coordinates of the observatory are 78.148°N, 16.043°E at an altitude of 520 m.

As of early 2024, the observatory contained over 25 optical instruments and 16 non-optical instruments. While the non-optical instruments can operate continuously, the optical instruments require varying levels of darkness and clear skies to make their observations. These instruments are placed underneath transparent domes (seen on the observatory roof in Fig. 1), which are heated to keep them free from snow and ice, so that the instruments have an unobstructed view of the sky. Types of instrumentation include: all-sky cameras, narrow field-of-view (FOV) imagers, spectrometers, photometers, interferometers, magnetometers, Global Navigation Satellite System (GNSS) receivers, and other radio and non-optical instruments. A virtual tour of the observatory is available online[1]. An international research community designs, builds, and maintains the instruments at KHO. As of early 2024, there are instruments from 18 institutions from 9 countries.

Although the site itself is maintained by a small, local crew, instrument principal investigators, and their teams visit frequently for instrument maintenance and upgrades. KHO is also used for teaching activities and as ground support for international campaigns involving sounding rockets. Figure 2 shows an overview of the different types of instruments at KHO, and their targeted altitude regions of the atmosphere. The instruments target the ionosphere, a region where solar radiation ionizes neutral particles, creating charged ions and free electrons. The ionosphere spans altitudes roughly between 60 and 1000 km and is partitioned into the D-,

[1] https://youtu.be/CVBNDK3UJVA

Fig. 1. A bird's eye view of the Kjell Henriksen Observatory. The two EISCAT Svalbard Radar antennas can be seen behind the observatory. The road through the Adventdalen valley is also visible, which leads to the town of Longyearbyen in the top left of the image. Image credit: Bjørn Strathmann.

Fig. 2. Overview of the types of instrumentation located at the Kjell Henriksen Observatory and their target altitude regions in the ionosphere. For a complete list of instruments see Appendix A.

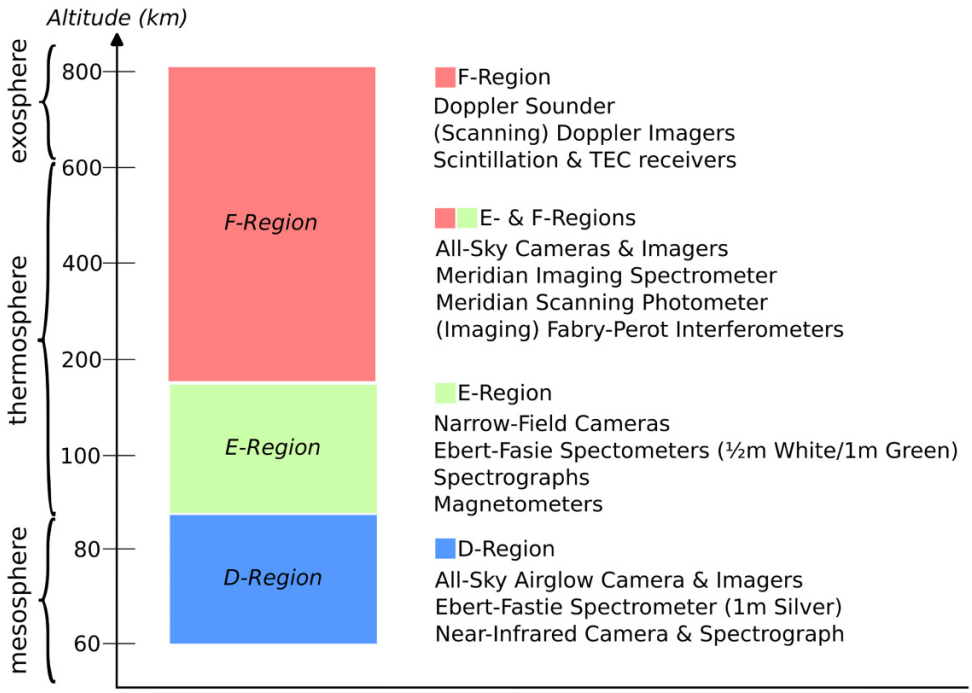

E-, and F-regions. Earth's magnetic field plays a crucial role in guiding, shaping, and controlling the motion of charged particles in the ionosphere. The instruments in the diagram have been placed in the regions where the majority of their measurements are concentrated. However, please note that there may be minor contributions from other regions. A list of all current instruments and their owners can be found in Appendix A. More detailed technical descriptions of the instruments can be found on the KHO website[2].

[2] http://kho.unis.no/Instruments.html

1.1. Space physics

The main focus of KHO is to gather data for space physics research, encompassing magnetic interactions between the Sun and Earth, and their consequences for the Earth's atmosphere. The Sun's magnetic field permeates the solar system, where it is known as the interplanetary magnetic field (IMF). The solar wind consists of charged particles that continuously stream from the Sun. The IMF is frozen-in to the outflowing solar wind, moving in sync with it. The Earth is shielded from the solar wind and IMF to an extent by its own magnetosphere, shown in Fig. 3. The magnetosphere is compressed on the dayside by the pressure from the solar wind,

Fig. 3. Illustration of the Earth's magnetosphere featuring a southward interplanetary magnetic field (IMF) depicted by yellow lines, draping around the magnetopause. Reconnection areas are denoted by grey boxes. Closed field lines are depicted in green, while open field lines are represented in purple. The directions of the magnetic fields are indicated by white arrows. Essential regions are labeled, and the orientation of the geocentric solar magnetospheric coordinate system is provided in the bottom left corner. Image credit: Katie Herlingshaw, based on Figure 1 of Burch et al. 2016 under the terms of the Creative Commons Attribution 4.0 International License (http://creativecommons.org/licenses/by/4.0/).

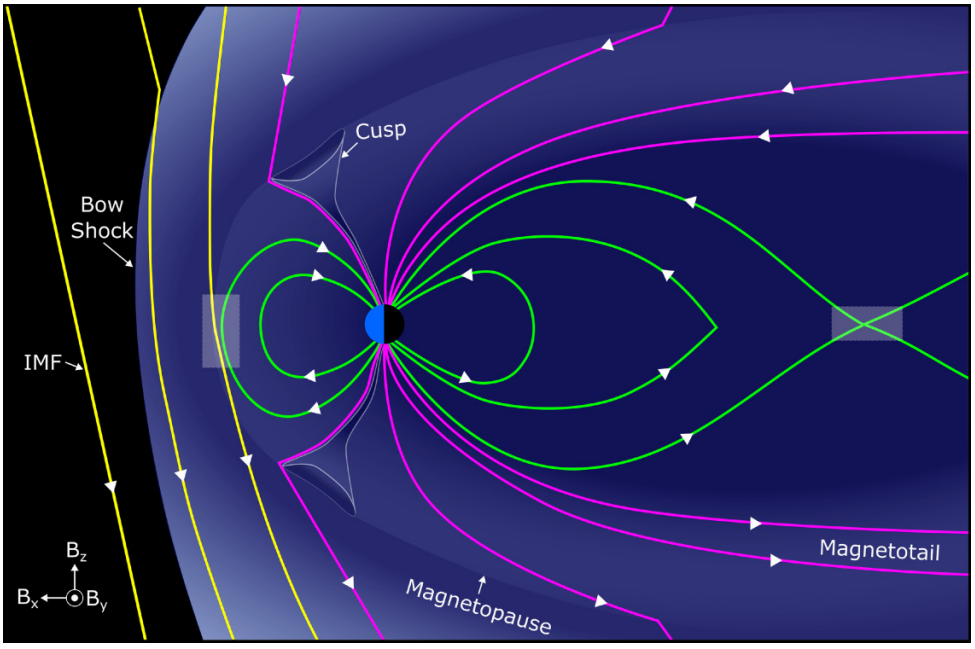

and stretched out on the nightside into a long magnetotail. This pressure balance forms dynamic boundaries such as the magnetopause and bow shock.

The orientation of the IMF dictates how it interacts with the Earth's magnetic field. The geocentric solar magnetospheric coordinate system is a framework used to describe the orientation of the IMF with respect to the Earth. The *X*-axis points from Earth towards the Sun, the *Z*-axis is the projection of the Earth's magnetic dipole axis on to the plane perpendicular to the *X*-axis (positive North), and the *Y*-axis completes the right-handed set (positive towards dusk). The IMF Bz component is often referred to as northward (positive IMF Bz) and southward (negative IMF Bz). When the IMF is orientated in the opposite direction to Earth's magnetic field, a process called magnetic reconnection occurs (e.g., Milan et al. 2017). The IMF and Earth's field lines break and merge together, allowing plasma from the solar wind to enter the magnetosphere. During this process, Earth's magnetic field lines transition from being closed (connected to the Earth at both ends) to open (one end connected to Earth and the other connected to the IMF). Reconnection occurs at the low-latitude magnetopause for southwards IMF and in the high-latitude lobes for northwards IMF. Reconnection also happens in the Earth's magnetotail, where open field lines merge to create closed field lines. Figure 3 shows reconnection regions for a southward IMF and indicates the direction of the geocentric solar magnetospheric coordinate system.

Magnetic reconnection accelerates charged particles along Earth's magnetic field lines, where they collide with atmospheric particles near the polar regions. This interaction leads to energy transfer and the emission of light within the ionosphere, manifesting as aurora. For example, collisions between magnetospheric particles and atmospheric oxygen atoms cause the red (630.0 nm) emissions above ~200 km (Jackel et al. 2003) and the green (557.7 nm) emissions approximately between 100 and 200 km altitude (Whiter et al. 2023). Higher energy particles can interact with molecular nitrogen, causing blue (427.8 nm) or purple emissions (Whiter et al. 2023).

The auroral ovals are centered on the north and south magnetic poles, positioned close to the region where the magnetic field lines shift from being closed to open. This transition area, known as the open–closed boundary (OCB), marks the poleward boundary of the auroral oval to the polar cap—a typically dim region characterized by open field lines. The size of the auroral oval can be modeled and expressed using the Planetary K index (Kp) (Matzka et al. 2021), an activity index ranging from 0 to 9. Magnetospheric processes called substorms can trigger the expansion and brightening of the auroral oval, leading to vibrant auroral displays. It is important to note that optical emissions, such as airglow, can arise from processes other than aurora. Unlike aurora driven by collisions from precipitating particles, airglow stems from chemical processes induced by solar radiation in the upper atmosphere.

Fig. 4. (*a*) Model of a contracted auroral oval (Kp index 2) at 08:00 UTC. The polar cap, auroral oval, and open–closed boundary (OCB) are indicated. The auroral oval is coloured green apart from the cusp region, which is coloured red. The red dots show the locations of the geomagnetic north pole and Longyearbyen, Svalbard. The lightly shaded circular area around Svalbard shows the optical horizon, thus approximating the field-of-view of an all-sky camera located in Longyearbyen. Image credit: Aurora Forecast 3D App. (*b*) An all-sky image of the red-dominant dayside aurora. Image credit: The Kjell Henriksen Observatory.

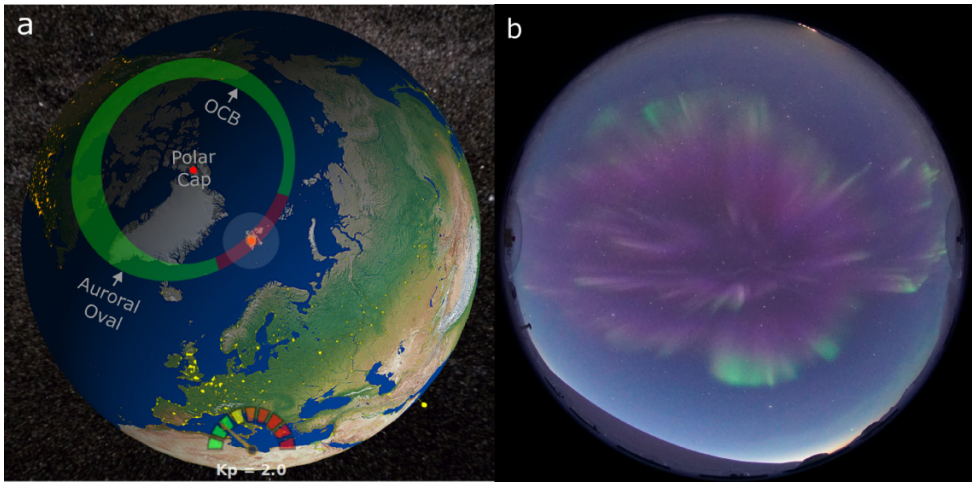

1.2. Svalbard's pivotal position for auroral research

Svalbard has a pivotal position for fundamental auroral research. Due to its location far above the Arctic Circle, there are several months each year where the Sun either does not set (midnight sun) or does not rise (polar night). During the latter period, from late November until late January, optical instrumentation can operate continuously (24/7) in a 2-month period surrounding the winter solstice (December 21). There are very few locations on dry land at such a high latitude in both the northern and southern hemispheres that have the infrastructure and accessibility offered by Longyearbyen, Svalbard. The town was originally established for coal mining in 1906 but has since expanded mainly due to increased tourism, research, and education. Nowadays, the population of Longyearbyen is approximately 2400, and there are daily commercial flights to and from mainland Norway.

In addition to its accessibility and extended dark season, Svalbard also offers another location benefit for auroral research. Figure 4*a* shows the position of Svalbard beneath a modelled auroral oval at 8 UTC for a Kp activity index of 2. The red part of the oval signifies the dayside 'cusp' aurora. The cusp regions, shown in Fig. 3, are where particles from the solar wind can be directly funneled down along the magnetic field and into the Earth's upper atmosphere around magnetic noon in both hemispheres. The particles do not accelerate significantly during this process and create low-energy precipitation and predominantly red aurora (630.0 nm), as seen in an all-sky image from KHO in Fig. 4*b*. An intriguing feature of the cusp is the doubling of density measured by the CHAMP satellite as it passed through the cusp (Lühr et al. 2004). Among other hypotheses, Carlson et al. (2012) proposed, supported by modelling, that a combination of low-energy (soft) precipitation with strong plasma flow could create sufficient heating and upwelling to explain this unexpected observation, which affects satellite drag at very low Earth observation heights.

Although the concept of the cusp has existed for a long time (Chapman and Ferraro 1933), it was not until 1971 that the first observational evidence of the cusp was collected with particle detectors onboard satellites (Frank 1971; Heikkila and Winningham 1971; Russell et al. 1971). Observations of the cusp aurora with ground-based instrumentation provides a novel vantage point to monitor the interaction of the solar wind, the magnetosphere, and the Earth's upper atmosphere over a wide area and with high temporal and spatial resolution. The time evolution of features can also be monitored as they travel across the polar cap, as can the boundary between the open and closed magnetic field lines. Statistically situated inside the polar cap, Svalbard is not always able to capture the nightside aurora, but the nightside aurora are frequently seen when the auroral oval is either contracted (low Kp index) or in connection with dynamic poleward expansions of the auroral oval during auroral substorms. All sky camera timelapse from KHO on 18 December 2017 00–08:30 UT is provided in Supplementary Material (S1). The timelapse demonstrates how the green-dominant nightside aurora switches to the red-dominant dayside aurora at approximately 06:15 UT. The dayside aurora is dynamic and includes transient green features such as poleward moving auroral forms (Subsection 2.1) and fragments (Subsection 7.1).

1.3. History of auroral research on Svalbard

Optical auroral research on Svalbard dates back to the 1800s. During the Swedish North Pole expedition in 1868, Prof. Selim Lemström made spectroscopic measurements of aurorae at several locations on Svalbard (Lemström 1868). During the International Polar Year (IPY) in 1882–83 Sweden established a station at Kapp Thordsen (Ekholm 1887). Here one of many objectives was to measure the altitude and

Fig. 5. Images of (*a*) the small hut and repurposed second world war anti-aircraft searchlight in Endalen (1978) and (*b*) the Auroral Station in Adventdalen. Image credit: The Kjell Henriksen Observatory.

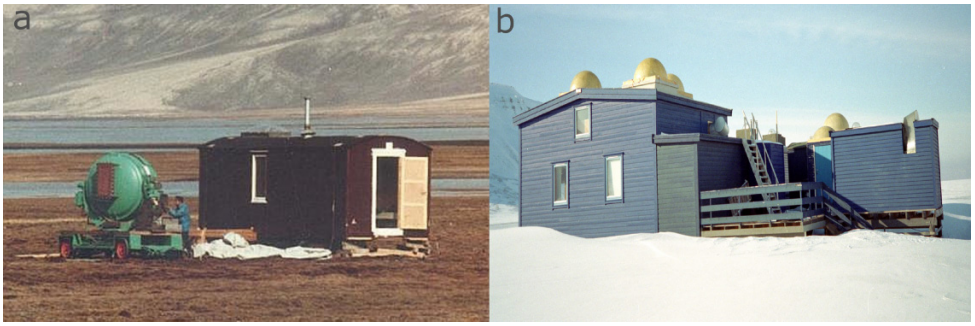

spectrum of the aurora. Although the IPY was a great success, equipment from that era lacked the sensitivity to reliably record the faint auroral light so the expedition had limited scientific impact. A new attempt was made by a Norwegian overwintering expedition in 1902–03, initiated by Kristian Birkeland (Birkeland 1908). Unfortunately, their cameras were still not advanced enough to photograph the faint and transient aurora effectively, and observations were primarily made under harsh circumstances from within a large barrel for the researchers to shelter from the cold winds (Lorentzen and Egeland 2011). Throughout the 1900s several recordings of the aurora and allied phenomena were performed on Svalbard, including at the Quade Hook meteorological station in the 1920s, at several locations during the 1932–33 IPY (Lindholm 1939) and, during the 1957–58 International Geophysical Year (Akasofu 1972). However, none of these observation campaigns became permanent.

This changed in 1966 with the establishment of the Ny-Ålesund research station, where the Auroral Observatory in Tromsø established a permanent presence with photometers, an all-sky camera, and a range of other instruments including an ozone spectrograph and riometers. However, the emphasis was still on the nightside aurora, so it served primarily as a northward expansion of the already well established auroral research activities performed on the Norwegian mainland. At the time, nobody realized the special vantage point under the cusp and the unique ability to make daytime, optical observations. However, with the great advancement in instrumentation after the International Geophysical Year and the advent of dayside auroral research in the early 1970s, the desire to establish long-term, targeted optical auroral observations from Svalbard was born.

The bold vision of establishing an optical auroral observatory in Longyearbyen was established through a collaboration between Professor Kjell Henriksen (University of Tromsø) and Drs. Abbas Sivjee and Chuck Deehr (both from University of Alaska). After funding was secured, a small prefabricated hut and a repurposed anti-aircraft searchlight system from World War II were chosen to house the auroral instruments, as shown in Fig. 5*a*. They were situated 7 km from Longyearbyen in the neighbouring valley, Endalen. The instruments included a spectrophotometer, a meridian scanning photometer (MSP), and a Fabry–Perot interferometer. These instruments were in operation from 1978 to 1983 during the Multi-national Svalbard Auroral Expedition. After this time, Henriksen led the effort to establish a permanent building in 1983, which they called the Auroral Station in Adventdalen. The Auroral Station, shown in Fig. 5*b*, became a hub for international auroral research and was used to collect the first systematic measurements of the dayside aurora between 1983 and 2007[3].

In 1993, the University Centre in Svalbard (UNIS) was established and immediately became involved in auroral research and operations at the Auroral Station in Adventdalen. However, the site faced challenges with inadequate space, a growing demand for new instruments, increased light pollution from Longyearbyen, increased traffic, and recurring sandstorms. In response to these challenges, Drs. Fred Sigernes and Dag Lorentzen secured funding to build a new, larger, and more modern observatory further away from Longyearbyen. They named this observatory in honour of Kjell Henriksen, in tribute to his devoted contributions to auroral research on Svalbard. The KHO facility is owned by UNIS and still in operation.

1.4. Research highlights from the Auroral Station

One specific dayside auroral signature is the 'proton aurora' (as opposed to the more famous 'electron aurora'), which is emission from hydrogen atoms from charge exchange with precipitating protons. This diffuse emission is caused by keV energy protons and measured at wavelengths of 656.3 and 486.1 nm and is emission from the Balmer series of atomic hydrogen. It is recognised as a direct footprint of dayside reconnection, where the proton energy increases with increased solar wind driving (Deehr et al. 1998). Significant efforts were put into modelling proton aurora to understand and characterise the phenomenon (Sigernes et al. 1993, 1994*a*, 1994*b*; Lorentzen 1999). Auroral Station spectrometer measurements were first used to compare with the model results and showed a reasonable agreement with the modelling work by Lorentzen et al. (1998). From the dayside reconnection site the newly opened magnetic field lines move

[3] More information on the history of KHO is available at https://kho.unis.no/History.html.

anti-sunward, which corresponds to poleward motion in the dayside ionosphere. Consistent with this motion, the proton precipitation energies were observed to decrease poleward (Holmes et al. 2009, 2011). This energy dispersion is called the velocity filter effect and was identified by comparing spectrometer data from the Auroral Station to spectrometer data from a site further north (Ny-Ålesund).

In the early 2000s, based on the first results of the High Throughput Imaging Echelle Spectrograph (HiTIES) instrument, Lanchester et al. (2003) described the energy and flux of protons from the ground-based spectral measurements and further showed an accurate agreement with results from the proton transport model. Furthermore, Ivchenko et al. (2004) showed that the proton precipitation can cause significant oxygen and nitrogen emissions (traditional electron aurora) in addition to the proton emissions.

One of the backbones of the dayside auroral studies based on data from the Auroral Station is the definition of the dayside OCB (Lorentzen et al. 1996). As cusp aurora gives a direct signature of the reconnection at the dayside magnetopause in the form of lower-energy electron precipitation, the equatorward boundary of this "soft" electron precipitation then marks the boundary between the open and closed magnetic field configuration. The equatorward boundary of auroral red emission, measured by the MSP, was shown to be the most precise way of detecting the OCB, and also, more specifically, shown to mark the boundary between the low latitude boundary layer (LLBL) and the boundary plasma sheet (Lorentzen and Moen 2000). The steepest gradient of the red emission intensity and its best suited mapping height was modelled by Johnsen et al. (2012) and validated by observations of Johnsen and Lorentzen (2012*b*). Thereafter, a statistical study on the dayside OCB location as a function of solar wind driving and geomagnetic activity was performed by Johnsen and Lorentzen (2012*a*) based on 15 years of MSP data, including the move of the instrument to its new housing at KHO. They noted that the average boundary location is at 75.4° magnetic latitude, and it correlates with geomagnetic indices and the solar wind energy input rate. MSP data using this technique, was also later used to validate auroral boundary determinations using mesoscale FAC identification from the CHAMP satellite (Xiong et al. 2014).

The manifestation of the dayside reconnection footpoint in the ionosphere is a newly opened energy transfer channel from the solar wind to the ionosphere. From Svalbard it allows us to follow the auroral structures that were seeded directly by reconnection, and are thus a means to indirectly study the dayside reconnection process itself. In addition to proton aurora, these phenomena also include poleward moving auroral forms (PMAFs) and polar cap patches (PCPs). An early statistical PMAF study by Fasel (1995) characterised the PMAF evolution and their relationship to solar wind driving. Moen et al. (1998) further mapped the particle precipitation of these moving auroral forms onto the open field lines of the LLBL, just poleward of the OCB.

The formation of PCPs was described in detail by Pryse et al. (2004) and Carlson et al. (2004, 2006). With multi-instrument observations they concluded that the enhanced F-region plasma source over Svalbard was photoionised in the upper atmosphere at lower latitudes in the afternoon. From there, the plasma migrates towards magnetic noon until it is brought anti-sunward across the OCB and into the polar cap. On the nightside, PCPs have been interpreted as tracers of reconnection and related to substorms at the end of their journey across the polar cap (Lorentzen et al. 2004). Newer highlights from the KHO era involving PMAFs and PCP will be discussed further in Subsections 2.1 and 2.2, respectively.

1.5. Coordination of co-located instrumentation

The KHO is not the only research infrastructure situated on the Breinosa mountain. Behind KHO in Fig. 1, the two antennas of the EISCAT Svalbard Radar (ESR) are visible. The dish on the left is 32 m in diameter and is fully steerable, while the other dish is 42 m in diameter and fixed along the magnetic field direction. Although the 32 m antenna is steerable, it is limited to elevations higher than or equal to 30°. The ESR operates in the 500 MHz band with a peak transmitter power of 1 MW. When operating at peak power, for example when the 32 m dish is in motion under wind resistance, the ESR uses approximately 20% of the total electrical power consumption from Longyearbyen town. The ESR has been in operation since 1996 and is capable of recording electron density and temperature in addition to ion temperature and line-of-sight ion velocity. The ESR has a small beam width of ∼1°, so despite the high spatial and temporal resolution, the ESR records a very localised measurement of these parameters across different altitudes in the ionosphere in the direction of the beam.

Furthermore, the Auroral Structure and Kinetics (ASK) instrument is co-located at the ESR site. ASK consists of three filtered imagers focusing on a narrow area around magnetic zenith, collecting data at a high temporal resolution to capture dynamic small-scale auroral features (e.g., Krcelic et al. 2024).

In addition, although not visible in Fig. 1, the Svalbard SuperDARN (Super Dual Auroral Radar Network) radar (Greenwald et al. 1995) is located approximately 500 m to the east of the ESR. This radar is part of an international network consisting of over 30 high-frequency (8–22 MHz) radars. Each radar has a large FOV spanning over 3000 km in range and 52° in azimuth. Individual radars can measure backscatter power, line-of-sight velocity, and spectral width. Measurements from all of the SuperDARN radars can be combined to produce maps of the high-latitude ionospheric convection in both hemispheres.

At the base of the Breinosa, in Adventdalen, is the SOUSY Svalbard radar. This facility, which is operated by Tromsø Geohysical Observatory (TGO) at UiT The Arctic University in Norway, consists of the SOUSY mesosphere–stratosphere–troposphere radar (Roettger 2000) and the Nippon/Norway Svalbard Meteor Radar (NSMR) (Hall et al. 2002). These two radar systems mainly probe the mesosphere and extract neutral winds, temperatures, and the presence of polar mesospheric summer echoes. The availability of the spectrographic measurements of neutral temperatures as obtained from KHO is valuable information to calibrate the meteor

radar. Since the establishment of UNIS, TGO has operated a flux-gate magnetometer at the Auroral Station and later KHO. This instrument is part of the greater International Monitor for Auroral Geomagnetic Effects (IMAGE) network of magnetometers (Viljanen and Häkkinen 1997) covering sub-auroral, auroral, cusp, and polar cap latitudes across the Nordic countries. Recently, Hall and Johnsen (2020, 2021) showed, by combining data from the magnetometer and the NSMR, how the mesospheric temperature estimates from meteor radars are affected by the ionospheric electrodynamics and how to correct for it.

The co-location of these instruments provides a larger-scale context to optical features observed in both all-sky cameras and narrow FOV cameras. In this way, fine-scale auroral structure and dynamics can be studied with optical instrumentation, while radar measurements provide information about ionospheric parameters and large-scale ionospheric convection. KHO-based optics and radar measurements from ESR and SuperDARN offer valuable insights individually, but their combined use can yield even more significant scientific output (Oksavik et al. 2004, 2005; Lorentzen et al. 2007, 2010; Barthélémy et al. 2011; Taguchi et al. 2015*b*; Thomas et al. 2015; van der Meeren et al. 2015, 2016; Chen et al. 2016; Hosokawa et al. 2016*b*; Kim et al. 2017; Kwagala et al. 2017; Herlingshaw et al. 2019; Price et al. 2019; Billett et al. 2020; Reidy et al. 2020; Belakhovsky et al. 2021; Dreyer et al. 2021; Whiter et al. 2021; Baddeley et al. 2023; Eriksen et al. 2023; Krcelic et al. 2023). The introduction of newer co-located instrumentation has allowed the comparison of different phenomena across diverse types of data. For example, a study by Chen et al. (2015) used the optically determined OCB as a ground truth in validating the spectral width boundary, which is claimed to identify the same boundary location based on High-Frequency (HF) SuperDARN radar data. An average poleward dislocation of spectral width boundary with respect to OCB of about 1° of latitude was explained by uncertainties in the HF backscatter locations in the ionosphere.

Ny-Ålesund, Barentsburg, and Hornsund are the other settlements on Svalbard that house optical instrumentation and other relevant infrastructure. Ny-Ålesund is located ∼120 km north of Longyearbyen and is one of two sounding rocket launch sites operated by Andøya Space, with the other located at Andøya itself. Sounding rockets are the only means of making in-situ measurements within the altitude range situated between the maximum weather balloon altitude (about 30 km) and the minimum satellite altitude (about 170 km, although it is uncommon for satellites to stay in orbit for an extended time below 400 km). Rocket trajectories can be carefully planned to a high precision, which allows targeted data acquisition from specific ionospheric layers or features (Moen et al. 2012; Oksavik et al. 2012; Lund et al. 2012; Lessard et al. 2020; Moser et al. 2021; Spicher et al. 2022).

For instance, by combining ground-based photometer measurements with the SCIFER rocket particle measurements, Lorentzen et al. (1996) and Sigernes et al. (1996) showed a good agreement between auroral emission heights and energies of the precipitating auroral electrons. KHO serves as a crucial scientific support location for rocket campaigns and KHO instruments have played a key role when determining optimal launch timing. Many rockets have been launched over Svalbard by Andøya Space but, until recently, they mostly consisted of isolated missions rather than coordinated efforts. The Grand Challenge Initiate (GCI)-Cusp project, involving multiple rockets, was developed to study the multi-scale physics of heating and auroral particle precipitation within the cusp. The GCI was an international endeavour, with 12 rockets in total spread over 9 different missions that were launched between 2018 and 2021. These rockets provided valuable insights into waves, instabilities, and neutral winds in the cusp and selected papers utilizing KHO data will be highlighted in more detail in later sections. As the GCI-Cusp was a success, a new multi-rocket collaboration is scheduled to capitalize on the upcoming solar maximum from 2024 onwards called GCI-3.0 Cusp Solar Max in which KHO will continue to provide ground support.

Beyond their role in supporting rocket campaigns, the instrumentation in Ny-Ålesund offers complementary data to that found at KHO. This includes all-sky imagers, riometers, photometers, and GNSS receivers, which study ionospheric and space physics processes over Svalbard (e.g., De Franceschi et al. 2019). These instruments are sometimes also part of extended networks covering larger areas of the Arctic region. Data from different sites can be combined and used for purposes such as triangulation and tracking of ionospheric features over the polar cap. It is also beneficial to compare Artic-based data to similar Antarctic data to investigate hemispherical symmetries and asymmetries between the polar hemisphere regions. While this paper focuses on scientific highlights specifically from KHO, it is important to acknowledge that KHO exists within a larger array of polar scientific infrastructure that can be used together to provide a more comprehensive picture of ionospheric and space processes (see e.g., Alfonsi et al. 2022).

2. Transient and travelling phenomena

Svalbard statistically passes underneath the cusp region on the dayside and is otherwise situated inside the polar cap or near the OCB. However, as the auroral oval is a dynamic and expanding area, it is also possible to obtain measurements of the nightside, morning, and afternoon sections of the oval from KHO. This makes KHO an ideal location to study how different features are created and destroyed by reconnection in addition to how they move on their journey across the polar cap. Monitoring the temporal and spatial evolution of ionospheric features can provide information about large areas of the magnetosphere that are currently inaccessible to in-situ spacecraft measurements with similar resolution.

In corrected geomagnetic coordinates, KHO is located at a latitude of 75.95° and a longitude of 107.23°. The coordinates were calculated using the International Geomagnetic Reference Field model with the current epoch (2020.0) and calculated for the year 2024. The KHO building is aligned with the meridian of the geomagnetic pole, positioned 32° west of the geographic north. When visualising locations in magnetic coordinates, polar plots of magnetic latitude and magnetic local time (MLT) are commonly used. MLT is expressed in hours

Fig. 6. Plot adapted from Baddeley et al. (2023), centered on the northern magnetic pole in magnetic latitude and magnetic local time coordinates, where 12 is noon (toward the Sun), 00 is magnetic midnight, 06 is dawn and 18 is dusk. Possible locations for the cusp, poleward moving auroral forms (PMAFs), polar cap patches (PCPs), a polar cap arc (PCA), pulsating aurora (PsA), and the auroral oval are indicated. Blue lines indicate the flow of ionospheric convection in the F-region.

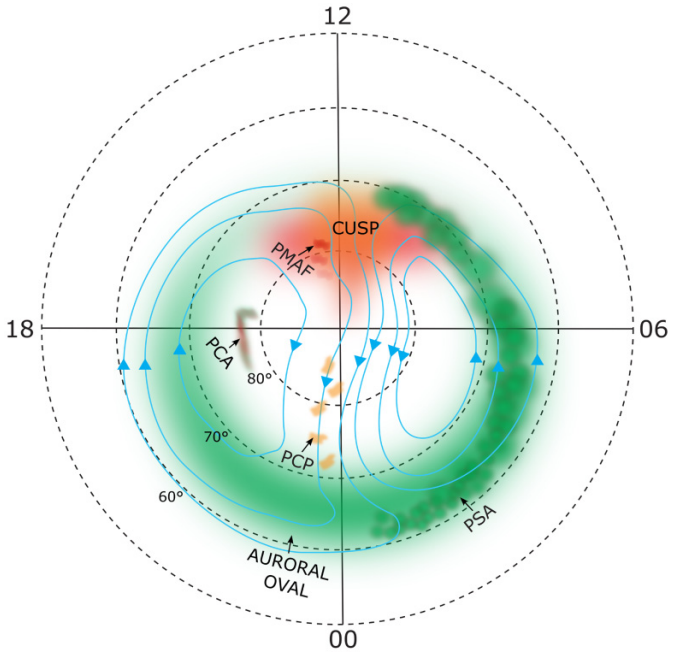

and ranges from 0–24, where 12 is magnetic noon and aligns with the direction of the Sun, 00 is magnetic midnight and is directed away from the Sun, and 06 and 18 point towards dawn and dusk, respectively. Figure 6 shows an example of this type of plot, providing possible locations of selected ionospheric features that will be discussed in the subsequent sections. The magnetic pole is at the center of the plot, and over the course of the day, KHO rotates through all magnetic local times at a magnetic latitude of 75.16°. KHO traverses magnetic noon at 08:47 UT and as a general the rule of thumb MLT = UT + 3 can be applied to calculate the MLT of KHO at a given UT.

2.1. Poleward moving auroral forms

PMAFs are discrete arc-like structures that form on the dayside auroral oval and then break away to drift into the polar cap. PMAFs are the optical ionospheric signatures of the dayside reconnection. Goertz et al. (2023) investigated the morphology of PMAFs using all-sky camera and MSP data located at KHO and presented their multi-stage evolution. This begins with an equatorward expansion and brightening of the auroral oval at the OCB. An arc then appears in the oval and moves poleward and possibly eastward/westward depending on the orientation of IMF By. The PMAF can brighten again, coincident with increases in auroral oval brightness, as it moves into the polar cap and eventually fades completely in all emission lines. Taguchi et al. (2015*b*) investigated the 3D structure of PMAFs by combining KHO all-sky imager (630.0 nm) data with ESR data recorded while the 32 m antenna was moving in elevation. The obtained 3D maps indicated the presence of a meso-scale twin-cell convection surrounding the PMAF, which had been predicted by the Southwood model (Southwood 1987). However, the symmetrical axis of the twin cells are inclined from the background flow by several tens of degrees. This method of producing 3D maps opens up unique possibilities for visualizing the meso-scale electrodynamics of the cusp.

Taguchi et al. (2015*a*) used 630.0 nm emissions from an all-sky imager at KHO and particle data from a spacecraft to study the particle precipitation features in the early and final stages of a PMAF. The spacecraft transited two PMAFs, one newly formed and one older. While both PMAFs had similar electron precipitation fluxes, the ion precipitation flux in the older one was much lower than in the newly formed PMAF. Due to this, it was suggested that the high flux of electron precipitation is controlled by a mechanism independent of the ion precipitation. It has also been suggested by Taguchi et al. (2012) that any individual PMAF may map to more than one burst of dayside reconnection. They also used all-sky images at the 630.0 nm emissions to observe that a single PMAF was comprised of two flow bursts within an interval of 2 min. This means that PMAFs may not have a one-to-one correspondent with reconnection bursts and that a single PMAF could comprise of multiple dayside reconnection bursts. Additionally, Burleigh et al. (2019) demonstrated the feasibility of using all-sky imager brightness data to constrain ionospheric model inputs. They examined the cumulative time-dependent impacts on ion upflow and downflow during a sequence of poleward moving auroral forms. Their method enabled the simulation of more realistic steady forcing validated using in-situ rocket measurements that is not captured by earlier simulations reliant on a stepwise on-off approach.

Studies of dayside reconnection usually focus on periods when the IMF Bz component is southwards, as then the low-latitude dayside reconnection occurs most effectively. Studying PMAFs under different IMF conditions can offer insights into the dayside reconnection at other locations in the magnetosphere including in high-latitude magnetospheric lobes. Li et al. (2021) showed an example of a PMAF forming under radial IMF due to dayside reconnection. A combination of all-sky images taken at KHO, SuperDARN ionospheric convection, magnetometer, and satellite data suggest that both low-latitude dayside and high-latitude lobe reconnection can occur simultaneously for radial IMF. Fasel et al. (2022) observed ionospheric signatures of reconnection during a northwards directed IMF using a sequence of all-sky camera images from KHO. They observed that as the IMF Bz component turned sharply northward, a series of discrete auroral forms propagated eastwards, aligning in the north–south direction after formation and then rotating clockwise during their eastwards drift. They named these features eastward-moving auroral forms and suggest that high-latitude reconnection is the mechanism behind the features.

2.2. Polar cap patches

As mentioned in Subsection 1.4, PCPs are polar cap phenomena that drift with the background ionospheric convection (Oksavik et al. 2010; Nishimura et al. 2014; Thomas et al. 2015). The combination of optical data from the MSP and an all-sky imager located at KHO, along with ESR and the ICI-2 sounding rocket data, was used in Lorentzen et al. (2010) to reveal that PCPs can be generated by a combination of increased density plasma from a sunlit ionosphere and precipitation in PMAFs. The formation of these patches has been observed to take place in a period of 5–10 min (Carlson et al. 2004, 2006), but longer periods of around 40 min have also been observed (Hosokawa et al. 2013*a*). The longer duration could potentially be explained by multiple processes occurring simultaneously on the dayside and giving rise to the PCP, which is an alternative process other than the typical explanation of PMAFs existing from transient reconnection events on the dayside.

Hosokawa et al. (2019) demonstrated that a low-cost all-sky camera is a viable tool for PCP research, although it has a lower radiometric resolution than a more sensitive camera. However, high camera sensitivity can be positive when researching patches, for instance, as seen in Hosokawa et al. (2016*b*) where they investigated newly formed 'baby patches'. The patches were observed to have airglow emissions of 100–150 R, which is lower than the luminosity of typical patches seen in the nightside polar cap. The authors suggested that this could be due to PMAFs creating patches with lower densities, which are still able to cause scintillation of signals from trans-ionospheric communication satellites (Oksavik et al. 2015).

Sakai et al. (2014) studied the 630.0 nm emission measured at KHO and ESR, as well as using atmospheric model data, to determine the volume emission rate of the patches (V_{630}). They discovered that increasing geomagnetic activity had an effect on the volume emission; namely, causing the the peak-altitude of V_{630} and the vertical extent of the emission layer to increase. They concluded that some of the enhanced emission could potentially be attributed to unstructured particle precipitation.

PCP plasma density and airglow emissions undergo changes as the patches transit the polar cap. Thomas et al. (2015) traced the signatures of PCPs through multiple instruments; SuperDARN, all-sky imagers, and total electron content (TEC) maps from GNSS. When PCPs arrive at the poleward edge of the nightside auroral oval, poleward boundary intensification has been observed, as seen in van der Meeren et al. (2015). They also reported severe scintillation in connection with auroral emission on the northern edge of the nightside oval. However, the low-density patches that left the polar cap at the time were not associated with strong scintillation. Another study investigating the connection between patches and nightside aurora was Jin et al. (2016). They studied the scintillation of 'auroral blobs' that were created by PCPs entering the nightside auroral oval. They found no correlation between preexisting scintillation associated with the patches and the enhanced scintillation that occurred when the blobs were created. The authors suggested that plasma dynamics response to auroral arcs could be responsible for the stronger scintillation and that the E-region conductivity could be a factor in the formation of the auroral blobs.

The edges of PCPs have been of great interest due to their association with high scintillation, as reported in Hosokawa et al. (2013*b*). Hosokawa et al. (2016*a*) investigated the leading and trailing edges of several traveling PCPs in the nightside auroral oval. The intensity gradient at the leading edge was found to be up to three times greater than at the trailing edge. Gradient drift instability was considered as the cause of the difference in the two gradients. Additionally, some of the patches showed finger-like structures at their trailing edges, which is also believed to be the result of growing gradient drift instability. In Hosokawa et al. (2013*b*) the finger-like structures were found to have a scale-size between 50 and 100 km, compared to the patch scale-size that was around 150 km. They found that the fingers 'grew' from the patch over a period of 5 min. Later, Hosokawa et al. (2014) observed patches with a dusk-dawnward extent of 1500 km and a north–southward extent of less than 500 km, resulting in a cigar-shaped patch. The variation in spatial extent (between 150 and 1500 km) and shape observed in the patches could be explained by the patches being created during different periods of geomagnetic activity (Thomas et al. 2015).

2.3. Polar cap arcs

Away from the bright auroral oval, the polar caps are typically thought to be dim, quiet regions. However, in addition to drifting PCPs, the darkness of the polar cap can also be interrupted by the presence of polar cap arcs (PCAs). These arcs tend to appear during periods of quiet geomagnetic activity or northwards directed IMF (van der Meeren et al. 2016; Hosokawa et al. 2020). For some time, the topology of the magnetic field lines that map to these arcs has been a controversial topic. It has been debated whether the arcs occur on the open field lines of the polar cap, closed field lines along the edge of the oval, or closed field lines that have protruded into the polar cap (Fear and Milan 2012).

Relatively little investigation has been undertaken into the small-scale features of PCAs. To address this, Reidy et al. (2020) presented the first observations of PCAs using ASK data on small scales in the order of meters with a millisecond–second temporal resolution. ASK data showed that one PCA occurred on closed field lines and was associated with dynamic, structured aurora while the other was on open field lines and had much less structure and lower fluxes. All-sky camera data were used to observe the larger scale evolution of the PCAs. Proton precipitation was observed by ground-based instrumentation during the PCA on closed field lines but not during the PCA on open field lines. These measurements were made by the HiTIES instrument, which is a part of the Spectrograph Imaging Facility at KHO. This observational data verifies criteria presented by Reidy et al. (2018) for identifying PCAs on open or closed field lines independently with HiTIES data.

Both Herlingshaw et al. (2019) and Reidy et al. (2020) observed flow channels on the edge of a PCA using SuperDARN data and all-sky camera data from KHO. Herlingshaw et al. (2019) found that the flow channel associated with the PCA

accounted for 60% of the cross polar cap potential, which is a proxy for the strength of the ionospheric convection. This suggests that flow channels are important features for the redistribution of flux over the polar cap. The PCA was a special kind known as a bending arc that form under IMF By-dominant conditions when IMF Bz is close to zero. Despite the lack of a substantial southwards IMF Bz component to drive the twin-cell convection over the polar cap, this study shows that flow channels can form and move plasma over the polar cap under dominant IMF By conditions (Herlingshaw et al. 2020, 2022).

2.4. Pulsating aurora

One of the most complex auroral structures is pulsating aurora (PsA), which manifests itself as irregular and diffuse patch or arc-like structures that fluctuate in brightness and cover large areas. A pulsating aurora display may consist of many different pulsation frequencies, which are not reflected by magnetic pulsation frequencies observed on the ground. While a number of studies have investigated PsA within the main auroral oval region, little is known about the high-latitude PsA.

After some early observations of high-latitude PsA in 1960s and 1970s, Partamies et al. (2022*a*) reported on a solar cycle of statistics on PsA observations over Svalbard based on colour all-sky camera images from KHO. They concluded that except for one PsA event out of 68 events, the high-latitude PsA is of the amorphous type. This is a PsA sub-category, which includes no stable, trackable structures, but rather large arc-like patches that evolve quickly. This type of PsA is associated with lower average electron precipitation energy as compared to other PsA types. Over Svalbard PsA is more infrequent than at lower latitudes, the event lifetimes are longer, and the required magnetic activity level is lower. It is unclear what determines the structuring of the PsA, but it is associated with structures of cold plasma in the plasmasphere, from where the electron precipitation is delivered to the ionosphere by wave-particle interactions.

2.5. Auroral emission heights and morphology

The Finnish Meteorological Institute operated identical auroral all-sky cameras in Ny-Ålesund and KHO during the time period of 1999–2009. The cameras run on the same imaging mode with the same set of optical filters. This allowed triangulation studies of auroral peak emission heights over Svalbard, showing that green (557.7 nm) auroral heights at high latitudes occur 3–5 km higher at nighttime as compared to the main oval latitudes (Partamies et al. 2022*b*). While the average latitudes of the nightside auroral oval never see the aurora during the day, Svalbard stations give an average magnetic noon auroral emission height of 140 km, in a good agreement with early volume emission rate profile study by Sigernes et al. (1996). These findings are based on over 80 000 individual measurements. It was further noticed in that study that increased solar wind speed only reduces the auroral peak emission heights in the pre-midnight to early morning in MLT, while at lower latitudes it evenly affects all MLT sectors. Another automatic measure used by Partamies et al. (2022*b*) was the structural index called Arciness, which describes the complexity of auroral structures in an image based on the distribution of brightest pixels. Analysis of Arciness index for Svalbard data showed that the increase in solar wind speed drives consistently more complicated morphological structures in all MLT sectors. The dayside (9–13 MLT) Arciness is high (arc-like structures) for both slow and fast solar wind. One example of an auroral feature that contributes to the high daytime Arciness is PMAFs (Goertz et al. 2023), which appear very arc-like, particularly at the beginning of their evolution, despite them being driven by fast solar wind (>500 km/s).

3. Mesosphere—lower thermosphere winds and temperatures

3.1. Neutral winds

In ionospheric research, the neutral winds are often neglected due to a lack of colocated as well as co-temporal measurements (Sarris et al. 2020). However, neutral winds can severely alter electromagnetic energy transfer rates between the plasma population and neutral atmosphere, as well as change the altitudes of the energy deposition of the auroral particles, or shift the energy dissipation maxima into different MLT regions (Aikio et al. 2012). Neutral wind measurements can be obtained in the E- and F-region via stochastic inversion of incoherent scatter radar data but this requires beam swinging (Nygrén et al. 2011) and running these types of experiments is expensive and cannot be done continuously. Satellite drag provides another method to estimate cross-track neutral winds in the upper atmosphere (Liu et al. 2006; Sutton et al. 2012), but is limited to the heights of spacecraft orbits.

In order to provide both more continuous measurements of the neutral winds as well as at lower altitudes, ground-based optical instruments, such as Fabry–Perot Interferometers (FPIs), can be used, provided that it is sufficiently dark and cloud free. KHO hosts three classical FPIs, an all-sky FPI called the Scanning Doppler Imager (SCANDI), and, since October 2022, a fixed-gap narrow field-of-view FPI called the Hot Oxygen Doppler Imager (HODI). The latter will be discussed in more detail in Subsection 8.3. SCANDI is cross-calibrated with a classical FPI, and is able to determine the neutral winds and temperatures based on Doppler shifts and broadening of red airglow and auroral emission at 630.0 nm at heights around 240 km (or green at 557.7 nm ~110 km (Aruliah et al. 2010)).

The SCANDI instrument has been used in several research themes over the years including a study comparing thermospheric zonal wind measurements from the ground and those of the CHAMP spacecraft at 350–400 km (Aruliah et al. 2019). They found a factor of 1.5–2.0 difference between the two measurement types. This could be an indication that the neutral wind magnitudes from the CHAMP spacecraft are too large, or that there is a significant wind shear between the measured heights. Uncertainties of these measurement affect our current modelling skills of the upper atmosphere. Auroral particle precipitation induced atmospheric gravity waves have also been observed as neutral wind

enhancements in concert with motion of the aurora (Katamzi-Joseph et al. 2019).

Another key topic concerns the response time of neutral particles when driven by plasma, which is often assumed to be long, especially at high latitudes (Billett et al. 2019). Utilizing the location of SCANDI in the Finland (Hankasalmi) and Iceland (Pykkvibaer) SuperDARN radar FOV, Billett et al. (2019) concluded on a response time of 1–1.5 h. Especially in the presence of meso-scale auroral structures, such as PMAFs, the neutral response time for plasma motion in the cusp is reduced to minutes rather than hours, thus significantly changing the energy exchange between the particle populations (Billett et al. 2020). The neutral wind estimates from SCANDI have further contributed to improved Joule heating rates at small scales. In the E-region, significant meso-scale variations in the Joule heating were found using SCANDI and ESR (Kosch et al. 2011). In the F-region Krcelic et al. (2023) combined SCANDI and ASK data to show the importance of small-scale electric fields on Joule heating and the differences between local and global estimations. The measured smaller scale variability in the neutral winds and heating rates signals that the plasma–neutral interplay is much more dynamic in reality than what the current models can reproduce. It is therefore important to note that FPI data from KHO has already been included in the empirical high-latitude thermospheric wind model, HL-TWiM, which represents large-scale circulation in Arctic and Antarctic regions (Dhadly et al. 2019).

While the above mentioned studies have focused on the horizontal motion of the neutrals, it is equally interesting to investigate the vertical flows (Lessard et al. 2023). A particular concern is the upwelling that increases the air density at higher latitudes and is thus experienced as a satellite drag (Lühr et al. 2004; Lessard et al. 2020). While most ionospheric upwelling studies use direct incoherent scatter radar measurements, ground-optical observations of sunlit aurora have recently been shown to be an additional way to estimate the N_2 upwelling (Ellingsen et al. 2021).

3.2. Neutral temperatures

Closely related to the atmospheric heating rates is the neutral temperature variability in the atmosphere, which employs different processes at different altitude ranges. Short-term variability of mesospheric neutral temperature as estimated from the hydroxyl airglow spectra (see Section 6) was studied by Enengl et al. (2021) as a response to energetic electron precipitation (EEP). They observed a temperature decrease in connection to EEP events that showed increased ionisation at the upper mesosphere heights in the EISCAT incoherent scatter radar. These temperature anomalies only lasted for about 30 min, and were interpreted as thinning of the airglow layer rather than as absolute temperature changes. The authors concluded that EEP may not have a long-term effect on the mesospheric temperature, but that temperature changes caused by particle precipitation are soon evened out by dynamical variability.

Short-term variability of upper thermospheric temperatures on small horizontal spatial scales has also been demonstrated by Griffin et al. (2009) with a multi-instrument case study using the Advanced Composition Explorer satellite, and ground-based instruments around KHO, namely: SCANDI and FPI; the ESR and selected SuperDARN radars; and magnetometers. They studied the time and spatial evolution of an ion-neutral coupling event over the SCANDI field-of-view (a diameter of around 800 km at 250 km altitude). The neutral temperatures measured by SCANDI Doppler broadening showed changes of 100 K in 20 min and a horizontal temperature gradient of 50 K over the SCANDI field of view.

Higher up in the auroral E-region, recent results describe large neutral temperature increases in and around auroral emission structures, caused by auroral electrodynamics and auroral electron precipitation (Price et al. 2019). These observations from the HiTIES instrument revealed significant Joule heating adjacent to an auroral arc. Furthermore, more localised heating was measured within the arc associated with intense electron precipitation.

4. Waves

Waves and oscillations in the ionosphere serve as signatures of energy transfer from the magnetosphere and solar wind. The frequency, location in latitude and MLT, duration, and characteristics of the waves can be used to identify the different energy source regions and dominant physical processes. Wave observations in the ionosphere also provide a remote diagnostic tool for regions in the magnetosphere and solar wind, which are rarely measured directly. Whilst the vast majority of studies use ground magnetometer data, wave signatures observed by optics, radar and rockets add an extra dimension to the understanding of, for instance, energy dissipation, turbulence, and spatial structuring of plasma. In addition, the ability to accurately place the wave signatures in relation to various magnetospheric regions, such as the OCB and the cusp, has proved vital in expanding our understanding of how different processes manifest themselves in ionospheric wave signatures. As such, several instruments at KHO have been involved in studies of waves.

Electromagnetic ultra low frequency (ULF) waves are often catagorized using the International Association of Geomagnetism and Aeronomy Pc/Pi (continuous/irregular) scale, which extends from 5 Hz down to 1 mHz (periods of 0.2–900 s). Electromagnetic ion cyclotron (EMIC) waves have a frequency range of 0.1–5 Hz in the Pc1–Pc2 band. They are generated through ion cyclotron gyroresonance with anistropic ion populations. Their energy source is primarily the ring current and plasma sheet. However, satellite measurements indicate that the cusps are also a source of Pc1–Pc2 waves. Engebretson et al. (2009) used magnetometers and ASCs in Svalbard to show that even intense particle precipitation in the central cusp does not accompany with ground-observed magnetic pulsations. However, regions of enhanced particle precipitation at the poleward edge of the cusp can be associated with waves observed on the ground. This places the source region of the downward propagating Pc waves to the plasma mantle, which maps to the poleward edge of the cusp. The global significance of these events is demonstrated by

Engebretson et al. (2015), who reported an EMIC wave event that extended across nearly 12 h in MLT and lasted more than 8 h.

EMIC waves have been associated with travelling convection vortices (TCVs), which are large quasi-sinusoidal transients near the dayside magnetopause with frequencies in the Pc5 band. Ionospheric effects of TCVs include large-scale vortical flows and enhanced field-aligned currents (FACs). Engebretson et al. (2013) presented the first simultaneous observations of EMIC waves and precipitating energetic protons associated with a TCV at a close proximity (1–3° equatorward) to the OCB. Multiple satellite observations in the upstream solar wind and bow shock region indicated that a spontaneous hot flow anomaly, a bow shock related instability, may have triggered this event. Kim et al. (2017) further reported EMIC wave bursts and TCVs resulting from a compression of the dayside magnetopause. All-sky camera, EISCAT, and SCANDI measurements also indicated a divergence in the thermospheric neutral winds during the TCV which was interpreted as heating due to FACs.

A multi-instrument study by Baddeley et al. (2017) investigated equatorward propagating auroral arcs driven by a standing mode Pc5 Alfvén wave called a field line resonance. The combination of ground and space based data allowed the authors to conclude that the wave energy was dissipated through ionospheric Joule and/or frictional heating and auroral particle acceleration, supporting theoretical models by Wright et al. (2003). The wave occurred in the dusk ionosphere and had a westward (sunward) propagation direction suggesting a magnetospheric energy source in the form of a compressional fast mode wave propagating sunward from the magnetotail.

To further understand and quantify the energy dissipation of ULF waves, van Hazendonk et al. (2024) performed a multi-instrument study using a combination of incoherent scatter radar, ground-based magnetometer, and all-sky imager data among others. The study found that the electromagnetic and kinetic flux can be of comparable magnitude for ULF wave events and should thus both be taken into account when quantifying energy dissipation of ULF waves.

Pilipenko et al. (2018) used observations of wave activity in the Pc5 and Pc6 band to determine that the source region for the broadband activity could not be associated with magnetopause surface eigenmodes as had been previously thought. The authors used the KHO MSP data to track the optical OCB and ground magnetometer data to determine the peak power of the Pc5 and Pc6 activity, located 2–3° equatorward of the OCB. This result places constraints on future models detailing dayside high latitude magnetic pulsations.

Yagova et al. (2017) used data from the KHO MSP and ground magnetometers to investigate whether Pc5/Pi3 pulsations (1–4 mHz) could be considered a pre-cursor to so called 'non-triggered' substorms. These are substorms occuring under quiet IMF conditions with no discernible IMF trigger (Hsu and McPherron 2004). By comparing the spectral characteristics of the Pc5/Pi3 band the authors showed distinct differences between the wave activity in the pre-substorm hours in comparison to times where there were similar geomagneic and IMF conditions, which did not lead to a substorm.

Very low frequency (VLF) waves in the 15–30 kHz range include auroral hiss, which is a radio emission associated with low energy (<100 eV) auroral electron precipitation. Satellites and rockets often observe so called 'VLF saucers' in the auroral hiss emissions. These are multiple V-shaped patterns in frequency–time spectrogram, and imply an unusually stationary source region either above or below the satellite. Moser et al. (2021) provided the first observations of large-scale VLF saucers associated with the cusp using electric field and electron detectors on board the CAPER-2 sounding rocket in conjunction with KHO all-sky camera, SuperDARN and EISCAT radar data. The authors showed that the VLF saucers originated from ∼4000 km altitude in the cusp and that the electron acceleration region was either above or in the same altitude range as the saucers.

5. Plasma irregularities and turbulence

Ionospheric plasma is known to be highly irregular, with fluctuations evolving both in space and time. These irregularities are common both in the equatorial and polar ionosphere regions, and cover a wide range of scales in the order of hundreds of kilometers down to to a few meters. The ionospheric cusps are well known regions of irregularities (Moen et al. 2013), but the sources of the irregularities and turbulence are not well understood, especially for the smaller scales (Moen et al. 2012). Given the heightened human activity in the Arctic and thus reliance on communication and navigation, there is a growing significance in advancing our understanding and identification of the physical mechanisms responsible for creating ionospheric irregularities, which can disrupt GPS and communication signals in the ionosphere. The University of Bergen operates four GNSS recievers on Svalbard; in Longyearbyen (KHO), Ny-Ålesund, Hopen, and Bjørnøya. These instruments collect phase and amplitude scintillation and TEC data (Oksavik 2020). These measurements are commonly combined with co-located optical or radar measurements in addition to rocket measurements so that in situ plasma parameters can be studied in turbulence and irregularities in combination with e.g., optical auroral signatures (Enengl et al. 2023, 2024).

Fæhn Follestad et al. (2020) used GNSS receivers and satellite data on the hypothesis that the presence of filamentary FACs is an essential component for the creation of severe phase scintillations on the dayside during winter time. They analysed GNSS data during 22 coincident satellite overpasses and found that in all cases where severe scintillation was present, there were co-located filamentary FACs, whereas only 15 contained large-scale density gradients. This suggests that filamentary FACs are a key component for phase scintillations in the dayside auroral region and therefore have important implications for space weather impacts on satellite communication. Spicher et al. (2022) used measurements from the TRICE-2 rockets to provide new insights into the sources and behaviour of high-latitude ionospheric irregularities in the cusp. These rockets flew simultaneously at different altitudes so provided a unique opportunity to use data from spatially separated probes and for an interferometric analysis of ionospheric parameters and electrodynamics.

They presented the first in situ experimental evidence of decameter-scale density irregularities being frozen-in within the F-region cusp ionosphere, which is a core assumption for SuperDARN convection maps.

It is common practice to use power spectra to analyse measurements of turbulence, but different kinds of waves and instabilities can generate similar power spectra so it is not possible to determine the generation mechanism with this information alone. Spicher et al. (2015) analyzed data from the ICI-2 sounding rocket experiment in the high-latitude F-region ionosphere. All-sky imager data at KHO were used to identify regions of precipitation and different ionospheric features along the rocket's trajectory. Instead of power spectra alone they used bispectral analysis. This gives extra information about phase coupling and allows the differentiation between cases with in-phase wave forms (referred to as coherent structures) and nonlinear interaction of individual waves where the phases vary randomly (referred to as turbulence). Using these classifications, they found coherent structures on the trailing edge of a cold PCP whereas in enhanced density regions where particle precipitation was present more random turbulent behaviour was observed. Further experimental and modeling studies are needed to assess whether irregularity structures are commonly different in the presence of particle precipitation.

Jin et al. (2017) reported that the presence of PCPs and cusp aurora produces the highest GPS phase scintillation levels in comparison to cusp dynamics without PCPs and PCPs without cusp aurora. However, Oksavik et al. (2015) warned that PMAFs can also cause significant phase scintillation, showing that strong ionospheric irregularities are present that may cause more severe disturbances in the cusp ionosphere than PCPs. This suggests that the structured particle precipitation of a bright PMAF event is an important source for plasma irregularities. In addition, Spicher et al. (2020) found that strong GNSS phase scintillations can arise from enhanced flow channels within the cusp. They performed the first quantitative, nonlinear analysis suggesting the Kelvin Helmholtz instability, which occurs in the presence of flow shears, as a process involved in the irregularity generation. They showed that the Kelvin Helmholtz instability can relatively easily explain the creation of density irregularities within minutes. In contrast, van der Meeren et al. (2016) found that for the case of PCAs, no significant amplitude or phase scintillation is observed. This suggests that even with the intense precipitation within the arc, strong irregularities are prevented from forming due to the low density background of the polar cap.

High-density plasma is drawn into the polar cap through reconnection but is not always segmented into PCPs and can sometimes stretch across the polar cap in a long, continuous tongue of ionisation (TOI). Van Der Meeren et al. (2014) presented a multi-instrument study of TOI using all-sky camera measuring the 630.0 nm emissions along with data from the ESR and SuperDARN radar. They observed bursts of phase scintillation at the leading edge of the TOI with highly localized and variable structuring there, from scale sizes of decameters to kilometers. This scintillation and structuring was not present within or ahead of the TOI and was isolated to the leading edge. Buschmann et al. (2023) studied in situ rocket measurements from the SS-520-3 rocket, which was launched through the cusp, a PCP and a TOI. Their findings showed that the highest variation in density on all scale sizes were located on the leading edge of the TOI.

6. Long time series example: mesospheric temperatures

One of the key missions of KHO is the continued observations that already started at the Auroral Station in Adventdalen. Two of the longest time series are measurements of auroral emission intensities by MSP and measurements of hydroxyl (OH) airglow spectra by an Ebert–Fastie spectrometer (1 m Silver, for instrument description see Sigernes et al. (2003)). Both datasets started already in the 1980s. Although the early years of these time series were more sporadic, since late 1990s and particularly during the KHO era, the data coverage has been systematic throughout the winter seasons.

Spectral measurements of OH airglow have been routinely used to estimate the neutral temperature in the mesosphere. This can be done under the assumption that the excited OH molecules are in thermodynamical equilibrium with the surrounding air, meaning that the population on the excited state can be described by a Boltzmann distribution, which is dependent on the ambient air temperature. Therefore, the emission line intensity ratios can be fitted to a temperature dependent synthetic spectrum, which then outputs the best fit temperature (Sigernes et al. 2003). While the OH airglow layer resides around 87 km height on average, the winter mesosphere, particularly in the northern hemisphere, undergoes large dynamical variations, which can move the airglow layer up and down. This vertical movement leads to adiabatic cooling and heating, respectively. It is thus important that the interpretation of these data is not done in isolation but with the dynamical state of the polar mesosphere in mind, as demonstrated by Dyrland et al. (2010). Global warming, for instance, is expected to have a cooling effect in the mesosphere, provided that the absolute temperature changes could be isolated from the dynamical effects (Laštovička 2023). It is also anticipated that periods of extremely cold stratosphere, that are observed as intense red skies on Svalbard (Sigernes et al. 2005), may be associated with warm anomalies in the mesosphere. In these topics our long time series can become extremely valuable.

Results of the OH airglow temperature analysis for all winter seasons (November–February) from the very beginning of the time series in 1983 until the spring 2013 was performed by Holmen et al. (2014). It was concluded that there is no long-term trend for these winter season average temperatures. To illustrate this, Fig. 7 shows the full data series supplemented with the winter season average temperatures until spring 2023. Holmen et al. (2014) further investigated the dataset for correlations with the solar activity, and reported on a mesospheric temperature change of about 4 K per 100 solar flux units of the F10.7 cm radio flux. The same finding was more recently emphasised by Haaland et al. (2022).

Trends in monthly averaged mesospheric temperatures have been observed to be positive apart from December, but

Fig. 7. The full time series of hydroxyl airglow temperatures since 1983. Daily average temperatures are marked as small red dots and annual average temperatures as large black dots with the standard deviation as an error bar.

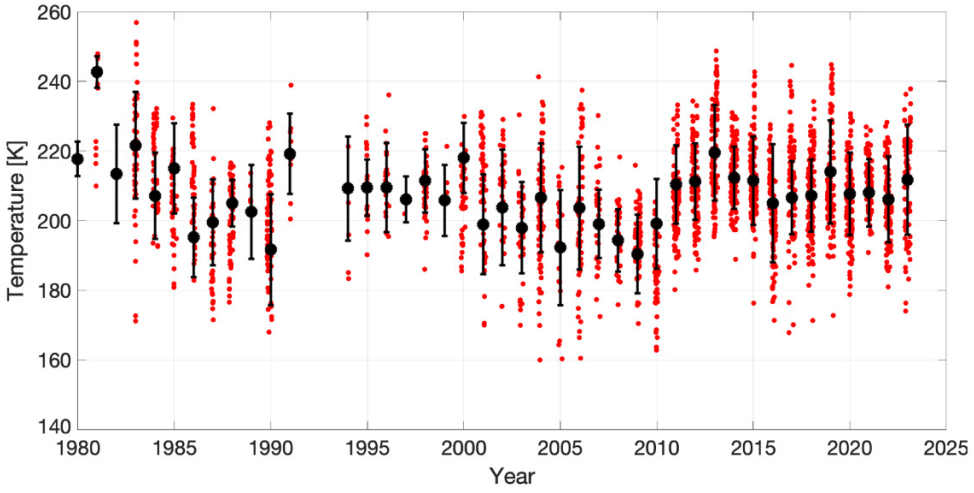

due to the dynamic driving of the temperature variability the confidence of any trends is generally very low (Holmen et al. 2014).

Spacecraft measurements of OH airglow layer height as well as ground-based observations of mesospheric winds are a key to understanding how much of the observed temperature changes on the long-term scale are due to dynamical variability. Independent all-year-round mesospheric temperature and wind measurements can be collected from the nearby meteor radar (NSMR) for comparison (Dyrland et al. 2010). Furthermore, KHO hosts guest instruments, which measure hydroxyl airglow emissions from different vibrational bands (UNIS spectrometer measures OH(6–2); HiTIES OH(8–3); Japanese spectrometer NIRAS-2 OH(8–5), OH(7–4), and OH(5–2), where the first number is the upper vibrational band and the second one the lower vibrational band). Different bands originate from slightly different heights (about 0.5 km per vibrational level; Von Savigny et al. 2012) and their spectral properties are different. By sharing and comparing our data, we can learn to better understand the OH airglow variability, the changes in the neutral temperature and the atmospheric wave properties and propagation. OH airglow data comparison requires that the temperature calculations have employed the same coefficients for the transition probability of the radiative decay. To facilitate this we have recently developed a conversion routine that does not require re-fitting of the raw spectra.[4]

Notably, the temperature analysis from the OH spectra collected by the HiTIES instrument includes modelling of the OH emission absorption by atmospheric water vapour, which is one of the key uncertainties in the spectral fitting. Quantifying the absorption of OH emission by water vapour enables estimates of the atmospheric water vapour content through as a side product (Chadney et al. 2017). This is a valuable data product the long-term atmospheric studies of the warming arctic, where the water content of the air is expected to rise.

7. Public outreach and teaching

The KHO also holds significance beyond its role as a scientific facility. A broad spectrum of visitors are welcomed for tours around KHO each year, where they gain valuable insights into the latest research. The Longyearbyen community can actively participate using their own auroral images. Students both from UNIS and the KHO partner institutions participate in fieldwork at KHO each year. The KHO observatory crew act as science ambassadors, communicating the importance of space physics research to a diverse audience in addition to educating the next generation of space researchers. Engaging with the media has provided an avenue to communicate research and has opened up opportunities for collaborations between researchers and videographers. A notable example is the application of a novel image accumulation filter technique to video footage of the 2015 solar eclipse taken by the Norwegian Broadcasting Corporation (Sigernes et al. 2017). This technique enhances intense and blurry footage, enabling the distinction of features in the Sun's upper atmosphere during an eclipse.

7.1. Citizen science

Technological advancements have now reached a stage where auroral photographs taken using mobile phones and entry-level cameras can easily capture an array of auroral structures and phenomena. A significant portion of the population possesses these devices, creating an untapped global source of auroral observations. There are different international efforts in place to create databases of these observations, communicate and educate the photographers about different types of aurora, and to provide examples that can be used for the public to browse data and classify different images. Members of the public who voluntarily participate in

[4] This tool is available at https://pypi.org/project/oh-einstein-temp-convert/.

scientific research and contribute valuable information without formal training are known as citizen scientists.

Visually striking auroral features that show specific patterns or shapes are the most accessible for members of the public to identify. For example, seashell aurora observed above Svalbard resulting from the compression of the dayside magnetosphere (Briggs et al. 2020) would be an ideal candidate. One phenomena that has captured the attention of the public due to research and outreach are fragmented aurora-like emissions—or simply "fragments". Fragments are small (km-scale), features observed mainly in the green (557.7 nm) emissions that either form alone or in periodic chains. Fragments do not fit neatly into either of the categories of aurora or airglow. They are therefore classified as aurora-like features and it is suspected that they are formed by a local instability in the ionosphere, although the exact instability is still debated.

The first articles on fragments were only recently published in 2021. Dreyer et al. (2021) based their publication on research conducted during a master's thesis (Dreyer 2019) using data from KHO, ESR, and the ASK instrument. They observed emissions in the 557.7 and the 673.0 nm lines but not in the more energy-consuming 427.8 or the 777.4 nm lines. This suggests an upper threshold on the generation mechanism energy and, along with the observation that the fragments are thin in the field-aligned direction, excludes particle precipitation as the source of the fragments. Whiter et al. (2021) investigated the conditions required for different instability processes using all-sky images from KHO in addition to ESR and ASK data. One of the case studies in this paper was identified in ASK data by citizen scientists using the online Aurora Zoo classification project[5]. There are many unanswered questions about fragments intended to be addressed in the coming years. Through a combination of community lectures, blog, and social media posts, and national/international media coverage, the goal is to inspire more individuals to become citizen scientists who can provide additional data or classify existing data to help address the future research questions. An image showing an example of fragments taken by citizen scientist Sophie Cordon is shown in Fig. 8.

7.2. Education

Several courses offered by the Arctic Geophysics department at UNIS provide students with fieldwork experience at KHO. Students participate in the annual calibrations of three spectrometers and the MSP. After completing the calibration activity, Raphael Deirmendjian created an instructional document[6] and video[7] to explain the process of calibrating the 'Silver Bullet' spectrometer to future students. Master's students have also made substantial contributions to the scientific research output from KHO over the years (Briggs et al. 2020; Dreyer et al. 2021; Enengl et al. 2021; Goertz et al. 2023). Overall, students are integral to the calibration of instruments, the development of educational initiatives, and the ongoing research at KHO.

In addition to the specialized education of bachelor's, master's, and PhD level students, UNIS researchers also actively engage in public education. Guided tours at KHO have been attended by students at Longyearbyen school, politicians, artists, authors, comedians, local guides, and many more. Realtime data from the KHO all-sky cameras are broadcast in various hotels and establishments to be used by the public, guides in the tourism industry, and local aurora enthusiasts. To assist aurora enthusiasts with pre-planning their observations, Sigernes et al. (2011) developed an app that allows users to check the aurora forecast, visualise their location relative to the modelled auroral oval, and view what percentage of the sky the aurora is predicted to cover and in which direction (as seen in Fig. 4*a*). A master's student project also improved the forecast available on the app by providing an oval model that consisted of separate approximations for the equatorward and poleward boundaries using empirical models on particle data from space-borne detectors (Breedveld 2020). The Aurora Forecast 3D app has over 50 000 active users with a very positive review averaging 4.3 out of 5.0. The app is believed to be popular mainly in the auroral tourism industry and in the amateur radio community. In addition the Norwegian Center for Space Weather at TGO is providing auroral forecasts based on this software through their webpages[8].

8. Instrumentation development and innovation

8.1. Meridian Imaging Svalbard Spectrograph

MSPs commonly use a moving mirror to scan the sky and reflect light through interference filters to photomultiplying tubes. This often results in rather large instruments. The KHO crew has developed a compact hyperspectral pushbroom imager, Meridian Imaging Svalbard Spectrograph (MISS), that captures the visible spectrum along the meridian. MISS uses a fish-eye lens followed by a north–south aligned slit, tunable transmission grating and prism, and an inexpensive cooled CCD-camera. No moving mirrors are needed as the captured hyperspectral image provides spectra along the meridian at roughly one degree angular resolution. Initial laboratory tests indicate a spectral resolution of the order of ~1 nm. MISS is currently operational at KHO. Figure 9 shows a comparison of MSP and MISS data for the same day and wavelengths. While a more thorough comparison including laboratory calibration of MISS is needed, the results are very encouraging. It is noteworthy that the MSP is automatically switched off to protect the photomultiplying tubes from bright moonlight (around noon as visible in Fig. 9) while this is not an issue for the CCD sensor of MISS.

8.2. Instruments for HYPSO-1/2/3 satellites

Development of hyperspectral imagers at KHO began in the early 2000s. Sigernes et al. (2000) developed a hyperspectral imager with grating-prism configuration. The work has

[5] https://www.zooniverse.org/projects/dwhiter/aurora-zoo
[6] http://kho.unis.no/doc/Silver_Bullet_Calibration_report.pdf
[7] https://www.youtube.com/watch?v=WP0HZCWyedU&ab channel =Raph%27

[8] https://site.uit.no/spaceweather/data-and-products/aurora/

Fig. 8. Image taken by citizen scientist Sophie Cordon in Longyearbyen showing fragments marked by red arrows.

Fig. 9. Comparison of Meridian Scanning Photometer (MSP) data in the top row to Meridian Imaging Svalbard Spectrograph (MISS) data in the bottom row on 1 December 2023. The plots show the scan in zenith angle from north to south over 1 day, where the colours indicate higher intensities of light in the 630 nm line (left column) and the 557.7 nm line (right column). The raw MISS data were manually scaled for visual comparison and no background subtraction was performed.

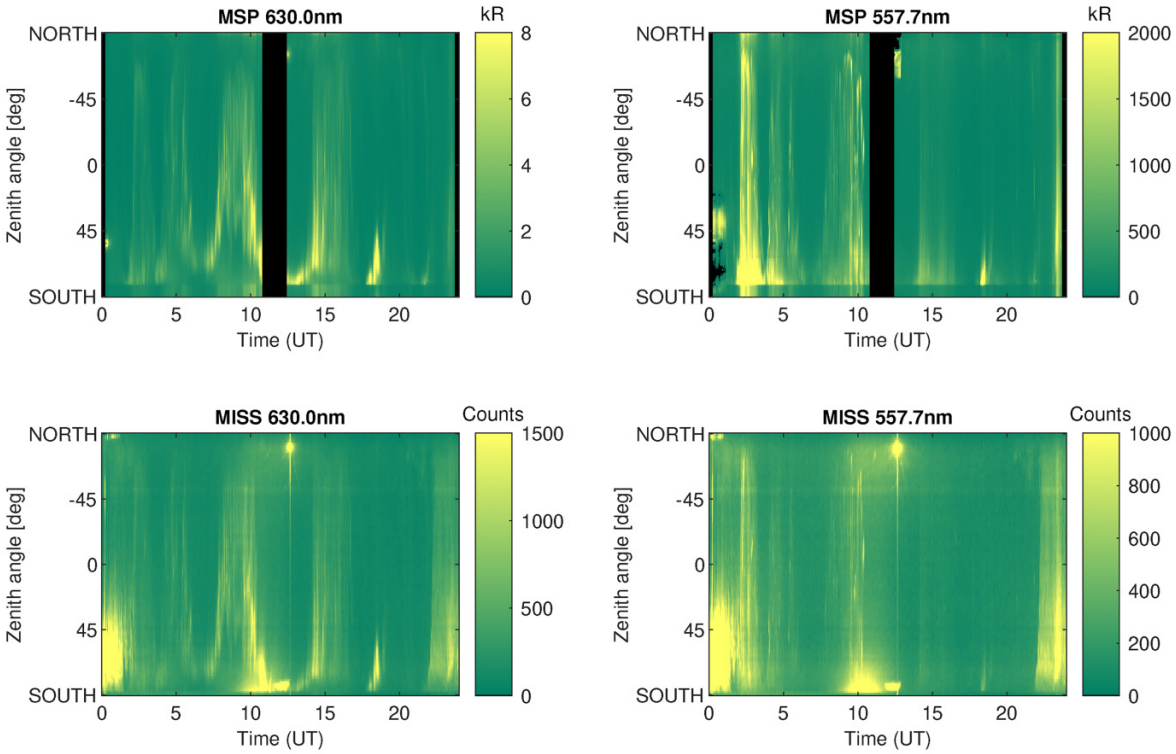

resulted in two instruments at KHO: the hyperspectral tracker and MISS. While the tracker is primarily designed for rocket campaigns, MISS is an excellent and compact candidate for next generation MSPs.

Another branch of the evolution of hyperspectral imagers includes much smaller imagers suitable for remote sensing applications. Sigernes et al. (2018) described a small, do-it-yourself hyperspectral imager that could be handheld or

flown with a drone. Henriksen et al. (2022) further improved the design, which eventually was selected as an instrument onboard the Hyperspectral Smallsat for Oceanographic Observations (HYPSO-1) satellite. The satellite was launched on 13 January 2022, and its mission is to monitor algal bloom based on ocean colour (Prentice et al. 2021; Bakken et al. 2023). An improved hyperspectral imager will be onboard HYPSO-2, whose launch is planned for 2024 (Berg et al. 2023).

Recently, the design of a new HYPSO-3 satellite has begun with three hyperspectral cameras as the payload. One of the cameras is identical to the flight-proven HYPSO-1 camera, while the second camera has an increased spatial resolution in the 400–800 nm wavelength region and the third one operates in the Near-Infrared region 700–1100 nm.

8.3. The hot oxygen Doppler imager

HODI is a fixed-gap narrow FOV Fabry–Perot interferometer. This instrument was designed for simultaneous observing of the particle velocity distributions of both ionized oxygen (732 nm) emission (e.g., Meriwether et al. 1978; Semeter 2003) and neutral thermospheric oxygen (630 nm) emission (e.g., Burnside et al. 1977; Gillies et al. 2017). HODI was deployed to KHO in October of 2022. The first season of observations from HODI showed many unique features, such as upflow in both the neutral and ionized oxygen in response to aurora. There is preliminary evidence of stronger upflow ($\sim$1000 m/s) co-located with the peak in the polar cap potential, but contamination by cloud cover makes the evidence currently inconclusive. Future observations will determine whether or not these speeds are ground truth.

HODI's ability to observe ions and neutrals from the same instrumental platform allows for near-simultaneous observations of the interactions in the ionosphere–thermosphere–magnetosphere system. HODI will continue making such observations at KHO, with three main goals in mind: further observation of upflows near the polar cap potential peak, investigation of the strong spike in densities seen by the Challenging Minisatellite Payload (CHAMP) satellite (Bruinsma and Forbes 2008), and quantification of the strength of the dynamic interaction of ions and neutrals in the auroral zone.

8.4. Advances in observations of short-wavelength infrared emissions

Cutting-edge short wavelength infrared (SWIR) imaging spectrograph (NIRAS-2) and monochromatic camera (NIRAC) were installed at KHO in late 2022 (Nishiyama et al. 2024). The measured SWIR molecular nitrogen ion band ($\sim$1.1 μm) is two orders brighter than the auroral blue emission at 427.8 nm, even with high temporal resolution (exposure times shorter than 30 s). Due to minimal contamination from resonant scattering (solar illumination -induced nitrogen emission), this band can be used to monitor auroral emissions even in twilight/sunlit conditions. This is an important improvement at high latitude regions, where twilight hours are longer than at mid and low latitudes. These measurements are facilitated by a new detector type that is particularly suitable for infrared wavelengths. The SWIR spectrograh provides high-resolution measurements of neutral temperature, and the SWIR camera complements the point measurements with two-dimensional images of the brightness perturbations in the airglow, which can then be used to derive parameters of the atmospheric waves.

Preliminary analysis of the new optical data together with electron densities measured by ESR have shown that the likely generation process for this SWIR band emission is impact excitation due to auroral electron precipitation in the lower E region (100–120 km). It is further suggested that the upper E-region emission is generated through charge exchange with oxygen ions. Another important aspect of the SWIR band is that it is utilised for sunlit aurora observations also from stratospheric balloons (Zhou et al. 2007). Continuous observations with the new ground-based instruments will undoubtedly provide important insights to support both balloon-based observations and future satellite-borne imaging in combination with our other ground-based observations.

8.5. Radio instrumentation

Two new radio instruments have been installed at the KHO: an ionosonde and a Doppler system. The ionosonde obtains an electron density profile of the E and lower F-region (up to the F-region density peak) above Svalbard using the simple relationship between plasma frequency and density. The KHO ionosonde is a newly designed system, developed in collaboration with UiT The Arctic University in Norway as the Master's project by Floer (2020). The goal of the project was to make a low-cost, easily reproducible scientific instrument. A particularly interesting feature is that the radio transmission power is very low being of the order or less than 1 W, which limits possible interference to any other nearby radio instruments. As such it uses commercially available, relatively inexpensive hardware along with a software-defined radio system. The operating and analysis software is also open source and is available through github[9].

The Polar Research Ionospheric Doppler Experiment is a bistatic radar system with a fixed frequency HF Continuous Wave transmitter located at the Stanisław Siedlecki Polish Polar Station in Hornsund and a receiver at the KHO. The system will detect small scale modulations in the ionospheric layers—such as those caused by ULF or Atmospheric Gravity Waves—using the Doppler effect. A system of this kind has not been successfully deployed on Svalbard before so this will be a new and exciting dataset. The initial data processing has now been completed as part of a Master's project by Cécily Noaillac[10].

9. Data availability and analysis advancements

Quicklook data for UNIS instruments are largely available through KHO web pages[11]. The colour image dataset used for the automatic morphological classification has been

[9] https://github.com/markusfloer/ionosonde
[10] https://aurora.unis.no/doc/ISAE_SUPAERO_Student_Project_Report_final.pdf
[11] http://kho.unis.no/Keograms/keograms.php

published through the Norwegian Research Data Archive (Partamies et al. 2023). We further plan to make all colour image data from Sony colour camera (used for classification purposes) available and browseable through the Canadian platform AuroraX[12]. This platform will allow inclusion of any image classification results. It also allows quick searching for conjunctions between ground stations and spacecraft overpasses, which will make future event selection hugely more efficient. The University in Bergen GNSS receiver data is available online (Oksavik 2020). In addition, the University of Oslo all-sky camera data is available online[13]. University College London provides real-time cloud sensor plots and all-sky camera images online[14]. The cloud sensor compares the ground and sky temperature to estimate clear sky conditions and has been validated with manually labelled all-sky images and weather measurements[15]. An archive is available since installation at KHO in January 2016. Future plans include making data available through the Svalbard Integrated Arctic Earth Observing System website[16].

Auroral imaging is producing too much data for studies that are solely based on visual inspection of images. Machine learning based methods should then be implemented for automatic sorting of KHO image data. Recently three master students have been involved in such projects using KHO data. Thus, there is currently a prototype for classifying full colour images into classes of *Aurora* and *No Aurora*, as well as a prototype method based on unsupervised learning that clusters images containing aurora into morphological classes.[17] Further analysis of the unsupervised learning results suggests that a sub-group of the morphological classes can be used to automatically detect auroral breakups in the image data (Partamies et al. 2023), which can become an asset in the future studies, in particular when the optical auroral activity is beneficial for analysis of other data types. Lastly, there are also some github repositories available with code that can be used to plot data from different instruments at KHO and other useful plots. Repositories beginning with 'KHO-' have been added for KHO users[18]. The magnetometer data from KHO is available through the TGO webpages[19] both with plotting and ASCII format (password on request). The magnetometer is part of the IMAGE network[20], where the data is included together with 57 other magnetometers covering Northern Europe, Jan Mayen, Iceland, and Eastern Greenland (as of 2024). IMAGE also provides the data to SuperMAG[21], which is a global repository for 1 min magnetometer data. Both IMAGE and SuperMAG have built in online tools to interpolate and calculate equivalent currents and delivers various geomagnetic activity indices. The latter also join the magnetometer data to global satellite imagery from the Polar spacecraft and the Imager for Magnetopause-to-Aurora Global Exploration (IMAGE) spacecraft. Care should be taken to differentiate between the IMAGE magnetometer chain and the IMAGE spacecraft as they share the same acronym. Both data sets (IMAGE and SuperMAG) are powerful repositories for applying offline tools such as GMAG (Murphy et al. 2022) and Local Mapping of Polar Ionospheric Electrodynamics (Hovland et al. 2022).

10. Conclusion

The research conducted at the KHO has played a key role in advancing our knowledge of different phenomena in the polar atmosphere. Functioning as the world's largest optical observatory for aurora and airglow processes, KHO has built upon the pioneering dayside observations from the Auroral Station in Adventdalen, leading to well-established climatological measurements, some of which now span over 40 years. The diverse range of instrumentation at KHO along with the co-location of other optical and radar instrumentation has fostered fruitful multi-instrument studies. Additionally, many satellites also complete polar orbits and can provide useful data over Svalbard including the energy, flux, and composition of precipitating particles as well as information about current systems, electric and magnetic fields, and ionospheric turbulence. Sounding rocket launches over Svalbard offer a unique opportunity for in situ measurements that can be combined with ground and satellite observations to provide comprehensive scientific insights into different ionospheric processes over multiple scale sizes. The existing network of instrumentation in such a unique location coupled with already established long-time series creates an ideal setting for the installation of new instrumentation. For example, Baddeley et al. (2023) suggest that the addition of a new phased array incoherent scatter radar would further enhance the capabilities of the research infrastructure.

The opportunity to install instrumentation underneath the dayside cusp region at KHO has attracted a wide range of international teams, fostering an excellent environment for global collaboration. Through this, KHO has also served as an accessible test-bed for instrument development featuring the installation of several promising new types of instrumentation both at the observatory and on board recently launched space missions. While the substantial volume of data from KHO provides a challenge for download and analysis, keyograms are available online for quick browsing and advances in auroral image classification show promise for filtering the data in the future.

Over the decades, auroral researchers on Svalbard have become culturally ingrained within the Longyearbyen community. While in the 70s and 80s, it was the auroral researchers and the coalminers that shared the town, the opening of The University Centre on Svalbard in 1993 marked a new era for research and education in Longyearbyen. UNIS students have played a key part in KHO research through their master's theses and also through instrument upkeep by undertaking the annual calibration of different spectrometers. In addition to the student community, KHO welcomes a diverse range of

[12] https://aurorax.space
[13] http://tid.uio.no/plasma/aurora/
[14] http://aplucl.uk/KHO.html
[15] https://kho.unis.no/doc/CloudSensorValidation.pdf
[16] https://sios-svalbard.org/
[17] Method is available at https://github.com/Tadlai/auroral-classification.
[18] https://github.com/orgs/UNISvalbard/repositories?type=all
[19] https://flux.phys.uit.no/geomag.html
[20] https://space.fmi.fi/image/www/index.php?
[21] https://supermag.jhuapl.edu/

visitors on tours of the observatory each year, from the Queen of Norway to local high school students. Communicating the research done at KHO and engaging citizen scientists to take part in auroral research is a priority for the observatory crew. This connection between the KHO research community and the broader public underscores the significance of KHO as a hub for both research excellence and public outreach.

Acknowledgements

The authors would like to thank the PIs of instruments at the Kjell Henriksen Observatory, with special thanks to Lasse Clausen, Satoshi Taguchi, and Peter Stauning for providing useful references for the article. Thank you to Sophie Cordon and Bjørn Strathmann for providing their photos for use in the article.

Article information

History dates

Received: 5 February 2024
Accepted: 16 August 2024
Accepted manuscript online: 17 October 2024
Version of record online: 3 February 2025

Notes

This paper is part of a collection entitled Thirty years of Earth System Science in high-Arctic Svalbard: status, trends, and future recommendations.

Copyright

Data availability

The data listed in this review paper are available within the references provided for the mentioned studies. Data that have not been previously published from the KHO include the time series of OH airglow temperatures from an Ebert–Fastie spectrometer and example keyograms from the Meridian Imaging Svalbard Spectrograph (MISS) and the Meridian Scanning Photometer (MSP). Quick look plots for the MISS and MSP are available online (http://kho.unis.no/Keograms/keograms.php) and full resolution data can be requested from instrument PIs Fred Sigernes (MISS, freds@unis.no) and Dag Lorentzen (MSP, dagl@unis.no). OH airglow temperatures from the Ebert–Fastie spectrometer are available on request from the instrument PI Fred Sigernes (freds@unis.no).

Author information

Author ORCIDs

Katie Herlingshaw https://orcid.org/0000-0001-6861-1914
Noora Partamies https://orcid.org/0000-0003-2536-9341
Charlotte M. van Hazendonk https://orcid.org/0000-0003-0156-9007
Mikko Syrjäsuo https://orcid.org/0000-0002-6113-6855
Lisa J. Baddeley https://orcid.org/0000-0003-1246-0488
Magnar G. Johnsen https://orcid.org/0000-0002-2776-0750
Nina K. Eriksen https://orcid.org/0000-0003-0008-3080
Anasuya Aruliah https://orcid.org/0000-0002-2849-8475
Mark J. Engebretson https://orcid.org/0000-0002-3882-8108
Kjellmar Oksavik https://orcid.org/0000-0003-4312-6992
Fred Sigernes https://orcid.org/0000-0002-7109-0424
Dag A. Lorentzen https://orcid.org/0000-0001-7628-4036
Takanori Nishiyama https://orcid.org/0000-0002-3648-6589
Matthew B. Cooper https://orcid.org/0000-0001-6137-8814
John Meriwether https://orcid.org/0000-0003-0826-1312
Stein Haaland https://orcid.org/0000-0002-1241-7570
Daniel Whiter https://orcid.org/0000-0001-7130-232X

Author contributions

Conceptualization: KH, NP
Data curation: NP
Methodology: KH, NP
Project administration: KH
Resources: KH
Software: MS
Visualization: KH, NP, MS, LB
Writing – original draft: KH, NP, C van H, MS, LB, NE, IM, AA, ME, TN, MC, JM, DW
Writing – review & editing: KH, NP, C van H, MS, LB, MJ, NE IM, AA, ME, KO, FS, DL, TN, SH

Competing interests

The authors declare there are no competing interests.

Funding information

Financial support was provided to Katie Herlingshaw by the Research Council of Norway under contract 343302.

Supplementary material

Supplementary data are available with the article at https://doi.org/10.1139/as-2024-0009.

References

Aikio, A.T., Cai, L., and Nygrén, T. 2012. Statistical distribution of height-integrated energy exchange rates in the ionosphere. Journal of Geophysical Research: Space Physics, **117**(10). doi:10.1029/2012JA018078.

Akasofu, S.I. 1972. Midday auroras and magnetospheric substorms. Journal of Geophysical Research: Space Physics, **77**(1): 244. doi:10.1029/JA077i001p00244.

Alfonsi, L., Bergeot, N., Cilliers, P.J., De Franceschi, G., Baddeley, L., Correia, E., et al. 2022. Review of environmental monitoring by means of radio waves in the polar regions: from atmosphere to geospace. Surveys in Geophysics, **43**(6): 1609–1698.

Aruliah, A., Förster, M., Hood, R., McWhirter, I., and Doornbos, E. 2019. Comparing high-latitude thermospheric winds from Fabry–Perot interferometer (FPI) and challenging mini-satellite payload (CHAMP) accelerometer measurements. Annales Geophysicae, **37**(6):1095–1120. doi:10.5194/angeo-37-1095-2019.

Aruliah, A., Griffin, E.M., Yiu, H.C., McWhirter, I., and Charalambous, A. 2010. SCANDI—an all-sky Doppler imager for studies of thermospheric spatial structure. Annales Geophysicae, **28**(2): 549–567. doi:10.5194/angeo-28-549-2010.

Baddeley, L., Lorentzen, D., Haaland, S., Heino, E., Mann, I., Miloch, W., et al. 2023. Space and atmospheric physics on Svalbard: a case for

continued incoherent scatter radar measurements under the cusp and in the polar cap boundary region. Progress in Earth and Planetary Science, **10**(1):53. doi:10.1186/s40645-023-00585-9.

Baddeley, L., Lorentzen, D.A., Partamies, N., Denig, M., Pilipenko, V.A., Oksavik, K., et al. 2017. Equatorward propagating auroral arcs driven by ULF wave activity: multipoint ground- and space-based observations in the dusk sector auroral oval. Journal of Geophysical Research: Space Physics, **122**(5): 5591–5605.

Bakken, S., Henriksen, M.B., Birkeland, R., Langer, D.D., Oudijk, A.E., Berg, S., et al. 2023. HYPSO-1 CubeSat: first images and in-orbit characterization. Remote Sensing, **15**(3):755. doi:10.3390/rs15030755.

Barthélémy, M., Lilensten, J., Pitout, F., Simon, W.C., Thissen, R., Lorentzen, D., et al. 2011. Polarisation in the auroral red line during coordinated EISCAT Svalbard Radar/optical experiments. Annales Geophysicae, **29**: 1101–1112. doi:10.5194/angeo-29-1101-2011.

Belakhovsky, V.B., Jin, Y., and Miloch, W.J. 2021. Influence of different types of ionospheric disturbances on GPS signals at polar latitudes. Annales Geophysicae, **39**(4):687–700. doi:10.5194/angeo-39-687-2021.

Berg, S., Bakken, S., Birkeland, R., Chiatante, C., Garrett, J.L., and Johansen, T.A. 2023. Ground systems software for automatic operation of the HYPSO-2 hyperspectral imaging satellite. *In* Sensors, systems, and next-generation satellites XXVII. *Edited by* T. Kimura, S.R. Babu and A. Hélière. SPIE, Amsterdam, the Netherlands. p. 40. doi:10.1117/12.2684263.

Billett, D.D., Hosokawa, K., Grocott, A., Wild, J.A., Aruliah, A.L., Ogawa, Y., et al. 2020. Multi-instrument observations of ion-neutral coupling in the dayside cusp. Geophysical Research Letters, **47**(4). doi:10.1029/2019GL085590.

Billett, D.D., Wild, J.A., Grocott, A., Aruliah, A.L., Ronksley, A.M., Walach, M.T., and Lester, M., 2019. Spatially resolved neutral wind response times during high geomagnetic activity above Svalbard. Journal of Geophysical Research: Space Physics, **124**(8): 6950–6960. doi:10.1029/2019JA026627.

Birkeland, K. 1908. The Norwegian Aurora Polaris Expedition 1902-1903 : Vol. 1 : on the cause of magnetic storms and the origin of terrestrial magnetism. Aschehoug, Christiania.

Breedveld, M. 2020. Predicting the auroral oval boundaries by means of polar operational environmental satellite particle precipitation data. Master's thesis, UiT The Arctic University of Norway, Department of Physics and Technology.

Briggs, J.K., Fasel, G.J., Silveira, M., Sibeck, D.G., Lin, Y., and Sigernes, F. 2020. Dayside auroral observation resulting from a rapid localized compression of the Earth's magnetic field. Geophysical Research Letters, **47**(19). doi:10.1029/2020GL088995.

Bruinsma, S.L., and Forbes, J.M. 2008. Medium- to large-scale density variability as observed by CHAMP. Space Weather, **6**(8). doi:10.1029/2008SW000411.

Burch, J.L., Moore, T.E., Torbert, R.B., and Giles, B.L. 2016. Magnetospheric multiscale overview and science objectives. Space Science Reviews, **199**: 5–21. doi:10.1007/s11214-015-0164-9.

Burleigh, M., Zettergren, M., Lynch, K., Lessard, M., Moen, J., Clausen, L., et al. 2019. Transient ionospheric upflow driven by poleward moving auroral forms observed during the rocket experiment for neutral upwelling 2 (renu2) campaign. Geophysical Research Letters, **46**(12): 6297–6305.

Burnside, R.G., Meriwether, J.W., and Torr, M.R. 1977. Contamination of ground-based measurements of OI (6300 Å) and NI (5200 Å) airglow by OH emissions. Planetary and Space Science, **25**(10): 985–988.

Buschmann, L.M., Bonnell, J.W., Bounds, S., Clausen, L.B., Kletzing, C., Marholm, S., et al. 2023. The role of particle precipitation on plasma structuring at different altitudes by in-situ measurements. Journal of Space Weather and Space Climate, **13**: 13.

Carlson, H.C., Moen, J., Oksavik, K., Nielsen, C.P., McCrea, I.W., Pedersen, T.R., and Gallop, P. 2006. Direct observations of injection events of subauroral plasma into the polar cap. Geophysical Research Letters, **33**(5). doi:10.1029/2005GL025230.

Carlson, H.C., Oksavik, K., Moen, J., and Pedersen, T. 2004. Ionospheric patch formation: direct measurements of the origin of a polar cap patch. Geophysical Research Letters, **31**(8).

Carlson, H.C., Spain, T., Aruliah, A., Skjaeveland, A., and Moen, J. 2012. First-principles physics of cusp/polar cap thermospheric disturbances. Geophysical Research Letters, **39**(19). doi:10.1029/2012GL053034.

Chadney, J.M., Whiter, D.K., and Lanchester, B.S. 2017. Effect of water vapour absorption on hydroxyl temperatures measured from Svalbard. Annales Geophysicae, **35**(3):481–491. doi:10.5194/angeo-35-481-2017.

Chapman, S., and Ferraro, V.C.A. 1933. A new theory of magnetic storms. Terrestrial Magnetism and Atmospheric Electricity, **38**(2):79–96. doi:10.1029/TE038i002p00079.

Chen, X.C., Lorentzen, D.A., Moen, J.I., Oksavik, K., and Baddeley, L.J. 2015. Simultaneous ground-based optical and HF radar observations of the ionospheric footprint of the open/closed field line boundary along the geomagnetic meridian. Journal of Geophysical Research: Space Physics, **120**(11): 9859–9874.

Chen, X.C., Lorentzen, D.A., Moen, J.I., Oksavik, K., Baddeley, L.J., and Lester, M. 2016. F region ionosphere effects on the mapping accuracy of SuperDARN HF radar echoes. Radio Science, **51**(5):490–506. doi:10.1002/2016RS005957.

De Franceschi, G., Spogli, L., Alfonsi, L., Romano, V., Cesaroni, C., and Hunstad, I. 2019. The ionospheric irregularities climatology over svalbard from solar cycle 23. Scientific Reports, **9**(1): 9232.

Deehr, C.S., Lorentzen, D.A., Sigernes, F., and Smith, R.W. 1998. Dayside auroral hydrogen emission as an aeronomic signature of magnetospheric boundary layer processes. Geophysical Research Letters, **25**(12): 2111–2114.

Dhadly, M.S., Emmert, J.T., Drob, D.P., Conde, M.G., Aruliah, A., Doornbos, E., et al. 2019. HL-TWiM empirical model of high-latitude upper thermospheric winds. Journal of Geophysical Research: Space Physics, **124**(12):10592–10618. doi:10.1029/2019JA027188.

Dreyer, J. 2019. A detailed study of auroral fragments. Master's thesis, Uppsala UniversityUppsala University, Department of Physics and Astronomy, Swedish Institute of Space Physics, Uppsala Division.

Dreyer, J., Partamies, N., Whiter, D., Ellingsen, P.G., Baddeley, L., and Buchert, S.C. 2021. Characteristics of fragmented aurora-like emissions (FAEs) observed on Svalbard. Annales Geophysicae, **39**(2): 277–288. doi:10.5194/angeo-39-277-2021.

Dyrland, M.E., Mulligan, F.J., Hall, C.M., Sigernes, F., Tsutsumi, M., and Deehr, C.S. 2010. Response of OH airglow temperatures to neutral air dynamics at 78°N, 16°E during the anomalous 2003–2004 winter. Journal of Geophysical Research Atmospheres, **115**(7). doi:10.1029/2009JD012726.

Ekholm, N. 1887. Observations faites au Cap Thordsen, Spitzberg, par L'Expédition Suédoise, Tome I: 1. Introduction Historique, Exploration Internationale des Régions Polaires 1882-1883.

Ellingsen, P.G., Lorentzen, D., Kenward, D., Hecht, J.H., Scott Evans, J., Sigernes, F., and Lessard, M. 2021. Observations of sunlit N2+aurora at high altitudes during the RENU2 flight. Annales Geophysicae, **39**(5): 849–859. doi:10.5194/angeo-39-849-2021.

Enengl, F., Kotova, D., Jin, Y., Clausen, L.B., and Miloch, W.J. 2023. Ionospheric plasma structuring in relation to auroral particle precipitation. Journal of Space Weather and Space Climate, **13**(4). doi:10.1051/swsc/2022038.

Enengl, F., Partamies, N., Ivchenko, N., and Baddeley, L. 2021. On the relationship of energetic particle precipitation and mesopause temperature. Annales Geophysicae, **39**(5): 795–809. doi:10.5194/angeo-39-795-2021.

Enengl, F., Spogli, L., Kotova, D., Jin, Y., Oksavik, K., Partamies, N., and Miloch, W.J. 2024. Investigation of ionospheric small-scale plasma structures associated with particle precipitation. Space Weather, **22**(1). doi:10.1029/2023SW003605.

Engebretson, M.J., Moen, J., Posch, J.L., Lu, F., Lessard, M.R., Kim, H., and Lorentzen, D.A. 2009. Searching for ULF signatures of the cusp: observations from search coil magnetometers and auroral imagers in Svalbard. Journal of Geophysical Research: Space Physics, **114**(A6).

Engebretson, M.J., Posch, J.L., Wygant, J.R., Kletzing, C.A., Lessard, M.R., Huang, C.L., et al. 2015. Van allen probes, noaa, goes, and ground observations of an intense emic wave event extending over 12 h in magnetic local time. Journal of Geophysical Research: Space Physics, **120**(7): 5465–5488.

Engebretson, M.J., Yeoman, T.K., Oksavik, K., Søraas, F., Sigernes, F., Moen, J.I., et al. 2013. Multi-instrument observations from Svalbard of a traveling convection vortex, electromagnetic ion cyclotron wave burst, and proton precipitation associated with a bow shock

instability. Journal of Geophysical Research: Space Physics, **118**(6): 2975–2997.

Eriksen, N.K., Lorentzen, D.A., Oksavik, K., Baddeley, L., Hosokawa, K., Shiokawa, K., et al. 2023. On the creation, depletion, and end of life of polar cap patches. Journal of Geophysical Research: Space Physics, **128**(12): e2023JA031739.

Fæhn Follestad, A., Herlingshaw, K., Ghadjari, H., Knudsen, D.J., McWilliams, K.A., Moen, J.I., et al. 2020. Dayside field-aligned current impacts on ionospheric irregularities. Geophysical Research Letters, **47**(11): 1–11.

Fasel, G.J. 1995. Dayside poleward moving auroral forms: a statistical study. Journal of Geophysical Research: Space Physics, **100**(A7): 11891–11905.

Fasel, G.J., Mann, J., Lee, L.C., Lee, S.H., Sigernes, F., Robison, A., and Tarditi, S. 2022. Northeastward-moving auroral forms from possible high-latitude reconnection. Journal of Geophysical Research: Space Physics, **127**(6).

Fear, R.C., and Milan, S.E. 2012. Ionospheric flows relating to transpolar arc formation. Journal of Geophysical Research: Space Physics, **117**(A9): 9230.

Floer, M. 2020. Design and implementation of a software defined ionosonde. A contribution to the development of distributed arrays of small instruments. Master's thesis, UiT The Arctic University of Norway, Department of Physics and Technology.

Frank, L.A. 1971. Plasma in the Earth's polar magnetosphere. Journal of Geophysical Research, **76**(22): 5202–5219. doi:10.1029/JA076i022p05202.

Gillies, D.M., Knudsen, D., Donovan, E., Jackel, B., Gillies, R., and Spanswick, E. 2017. Identifying the 630 nm auroral arc emission height: a comparison of the triangulation, FAC profile, and electron density methods. Journal of Geophysical Research: Space Physics, **122**(8): 8181–8197.

Goertz, A., Partamies, N., Whiter, D., and Baddeley, L. 2023. Morphological evolution and spatial profile changes of poleward moving auroral forms. Annales Geophysicae, **41**(1): 115–128.

Greenwald, R., Baker, K., Dudeney, J., Pinnock, M., Jones, T., Thomas, E., et al. 1995. Darn/superdarn: a global view of the dynamics of high-latitude convection. Space Science Reviews, **71**: 761–796. doi:10.1007/BF00751350.

Griffin, E.M., Aruliah, A., McWhirter, I., Yiu, H.I., and Charalambous, A. 2009. Upper thermospheric ion-neutral coupling from combined optical and radar experiments over Svalbard. Annales Geophysicae, doi:10.5194/angeo-27-4293-2009.

Haaland, S., Radlwimmer, A., van Schaik, B., Schillings, A., and Bjoland, L. 2022. Seasonal asymmetries and long- term trends in atmospheric and ionospheric temperatures in polar regions and their dependence on solar activity (SATS). In: M Gevers, et al. SESS Report 2022, Svalbard Integrated Arctic Earth Observing System. Longyearbyen. 26–44. doi:10.5281/zenodo.7371477.

Hall, C.M., and Johnsen, M.G. 2020. Influence of geomagnetic activity on derivation of temperatures from meteor wind radars. Radio Science, **55**(11): e07123.

Hall, C.M., and Johnsen, M.G. 2021. On the correction of temperatures derived from meteor wind radars due to geomagnetic activity. Experimental Results, **2**: e26.

Hall, C.M., Aso, T., and Tsutsumi, M. 2002. An examination of high latitude upper mesosphere dynamic stability using the Nippon/Norway Svalbard Meteor Radar. Geophysical Research Letters, **29**(8): 1280.

Heikkila, W., and Winningham, J. 1971. Penetration of magnetosheath plasma to low altitudes through the dayside magnetospheric cusps. Journal of Geophysical Research, **76**(4): 883–891. doi:10.1029/JA076i004p00883.

Henriksen, M.B., Prentice, E.F., Hazendonk, C.M.v., Hazendonk, C.M.v., Sigernes, F., Sigernes, F., and Johansen, T.A. 2022. Do-it-yourself VIS/NIR pushbroom hyperspectral imager with C-mount optics. Optics Continuum, **1**(2): 427–441.

Herlingshaw, K., Baddeley, L., Oksavik, K., Lorentzen, D.A., and Laundal, K.M. 2022. A statistical study of polar cap flow channels observed in both hemispheres using SuperDARN radars. Journal of Space Weather and Space Climate, **12**(11): 39. doi:10.1051/swsc/2022037.

Herlingshaw, K., Baddeley, L.J., Oksavik, K., and Lorentzen, D.A. 2020. A statistical study of polar cap flow channels and their IMF by dependence. Journal of Geophysical Research: Space Physics, **125**(11): e2020JA028359. doi:10.1029/2020JA028359.

Herlingshaw, K., Baddeley, L.J., Oksavik, K., Lorentzen, D.A., and Bland, E.C. 2019. A study of automatically detected flow channels in the polar cap ionosphere. Journal of Geophysical Research: Space Physics, **124**(11): 9430–9447. doi:10.1029/2019JA026916.

Holmen, S.E., Dyrland, M.E., and Sigernes, F. 2014. Long-term trends and the effect of solar cycle variations on mesospheric winter temperatures over Longyearbyen, Svalbard (78°N). Journal of Geophysical Research, **119**(11): 6596–6608. doi:10.1002/2013JD021195.

Holmes, J.M., Kozelov, B.V., Peters, N.J., Deehr, C.S., Lorentzen, D.A., and Sigernes, F. 2009. Ion velocity filter effect observed in dayside hydrogen aurora. Geophysical Research Letters, **36**(23). doi:10.1029/2009GL040972.

Holmes, J.M., Kozelov, B.V., Sigernes, F., Lorentzen, D.A., and Deehr, C.S. 2011. Dual site observations of dayside Doppler-shifted hydrogen profiles: preliminary results. Canadian Journal of Physics, **86**(5): 691–698. doi:10.1139/p08-026.

Hosokawa, K., Kullen, A., Milan, S., Reidy, J., Zou, Y., Frey, H.U., et al. 2020. Aurora in the polar cap: a review. Space Science Reviews, **216**(1): 15.

Hosokawa, K., Ogawa, Y., and Taguchi, S. 2019. Imaging of polar cap patches with a low-cost airglow camera: pilot observations in Svalbard, Norway. Earth, Planets and Space, **71**(1): 1–10.

Hosokawa, K., Taguchi, S., and Ogawa, Y. 2016a. Edge of polar cap patches. Journal of Geophysical Research: Space Physics, **121**(4): 3410–3420.

Hosokawa, K., Taguchi, S., and Ogawa, Y. 2016b. Periodic creation of polar cap patches from auroral transients in the cusp. Journal of Geophysical Research: Space Physics, **121**(6): 5639–5652.

Hosokawa, K., Taguchi, S., Ogawa, Y., and Aoki, T. 2013a. Periodicities of polar cap patches. Journal of Geophysical Research: Space Physics, **118**(1): 447–453. doi:10.1029/2012JA018165.

Hosokawa, K., Taguchi, S., Ogawa, Y., and Sakai, J. 2013b. Two-dimensional direct imaging of structuring of polar cap patches. Journal of Geophysical Research: Space Physics, **118**(10): 6536–6543.

Hosokawa, K., Taguchi, S., Shiokawa, K., Otsuka, Y., Ogawa, Y., and Nicolls, M. 2014. Global imaging of polar cap patches with dual airglow imagers. Geophysical Research Letters, **41**(1): 1–6.

Hovland, A.Ø., Laundal, K.M., Reistad, J.P., Hatch, S.M., Walker, S.J., Madelaire, M., and Ohma, A. 2022. The lompe code: a python toolbox for ionospheric data analysis. Frontiers in Astronomy and Space Sciences, **9**. doi:10.3389/fspas.2022.1025823.

Hsu, T.S., and McPherron, R.L. 2004. Average characteristics of triggered and nontriggered substorms. Journal of Geophysical Research: Space Physics, **109**(A7): 7208. doi:10.1029/2003JA009933.

Ivchenko, N., Galand, M., Lanchester, B.S., Rees, M.H., Lummerzheim, D., Furniss, I., and Fordham, J. 2004. Observation of O+ 4P-4D0 lines in proton aurora over Svalbard. Geophysical Research Letters, **31**(10).

Jackel, B.J., Creutzberg, F., Donovan, E.F., and Cogger, L.L. 2003. Triangulation of auroral red-line emission heights. In Proceedings of the 28th annual European meeting on atmospheric studies by optical methods, volume **92**. Sodankyla Geophysical Observatory Publications, Oulu, volume 92, pp. 97–100.

Jin, Y., Moen, J.I., Miloch, W.J., Clausen, L.B.N., and Oksavik, K. 2016. Statistical study of the GNSS phase scintillation associated with two types of auroral blobs. Journal of Geophysical Research: Space Physics, **121**(5): 4679–4697.

Jin, Y., Moen, J.I., Oksavik, K., Spicher, A., Clausen, L.B., and Miloch, W.J. 2017. GPS scintillations associated with cusp dynamics and polar cap patches. Journal of Space Weather and Space Climate, **7**: A23.

Johnsen, M.G., and Lorentzen, D.A. 2012a. A statistical analysis of the optical dayside open/closed field line boundary. Journal of Geophysical Research: Space Physics, **117**(A2): 2218.

Johnsen, M.G., and Lorentzen, D.A. 2012b. The dayside open/closed field line boundary as seen from space- and ground-based instrumentation. Journal of Geophysical Research: Space Physics, **117**(A3): 3320.

Johnsen, M.G., Lorentzen, D.A., Holmes, J.M., and Løvhaug, U.P. 2012. A model based method for obtaining the open/closed field line boundary from the cusp auroral 6300 Å[OI] red line. Journal of Geophysical Research: Space Physics, **117**(3).

Katamzi-Joseph, Z.T., Aruliah, A.L., Oksavik, K., Habarulema, J.B., Kauristie, K., and Kosch, M.J. 2019. Multi-instrument observations of large-scale atmospheric gravity waves/traveling ionospheric distur-

bances associated with enhanced auroral activity over Svalbard. Advances in Space Research, **63**(1): 270–281. doi:10.1016/j.asr.2018.08.042.

Kim, H., Lessard, M.R., Jones, S.L., Lynch, K.A., Fernandes, P.A., Aruliah, A.L., et al. 2017. Simultaneous observations of traveling convection vortices: Ionosphere-thermosphere coupling. Journal of Geophysical Research: Space Physics, **122**(5): 4943–4959. doi:10.1002/2017JA023904.

Kosch, M.J., Yiu, I., Anderson, C., Tsuda, T., Ogawa, Y., Nozawa, S., et al. 2011. Mesoscale observations of Joule heating near an auroral arc and ion-neutral collision frequency in the polar cap E region. Journal of Geophysical Research: Space Physics, **116**(A5): 5321.

Krcelic, P., Fear, R., Whiter, D., Lanchester, B., and Brindley, N. 2024. Variability in the electrodynamics of the small scale auroral arc. Journal of Geophysical Research: Space Physics, **129**(7): e2024JA032623.

Krcelic, P., Fear, R.C., Whiter, D., Lanchester, B., Aruliah, A.L., Lester, M., and Paxton, L. 2023. Fine-scale electric fields and Joule heating from observations of the aurora. Journal of Geophysical Research: Space Physics, **128**(2): e2022JA030628. doi:10.1029/2022JA030628.

Kwagala, N.K., Oksavik, K., Lorentzen, D.A., and Johnsen, M.G. 2017. On the contribution of thermal excitation to the total 630.0 nm emissions in the northern cusp ionosphere. Journal of Geophysical Research: Space Physics, **122**(1): 1234–1245. doi:10.1002/2016JA023366.

Lanchester, B.S., Galand, M., Robertson, S.C., Rees, M.H., Lummerzheim, D., Furniss, I., et al. 2003. High resolution measurements and modeling of auroral hydrogen emission line profiles. Annales Geophysicae, **21**(7): 1629–1643.

Laštovička, J. 2023. Progress in investigating long-term trends in the mesosphere, thermosphere, and ionosphere. Atmospheric Chemistry and Physics, **23**(10): 5783–5800. doi:10.5194/acp-23-5783-2023.

Lemström, S. 1868. Observations upon the electricity of the atmosphere and the 1541 aurora borealis, made during the swedish expedition of 1868 to the north pole. Smithsonian Institution, Washington.

Lessard, M.R., Damsell, A., Sadler, F.B., Oksavik, K., and Clausen, L. 2023. Interhemispheric asymmetries of neutral upwelling and ion upflow. Frontiers in Astronomy and Space Sciences, **10**. doi:10.3389/fspas.2023.1151016.

Lessard, M.R., Fritz, B., Sadler, B., Cohen, I., Kenward, D., Godbole, N., et al. 2020. Overview of the rocket experiment for neutral upwelling sounding rocket 2 (renu2). Geophysical Research Letters, **47**(21): e2018GL081885. doi:10.1029/2018GL081885.

Li, H.M., Shue, J.H., Taguchi, S., Nosé, M., Hosokawa, K., Ruohoniemi, J.M., et al. 2021. Dayside cusp aurorae and ionospheric convection under radial interplanetary magnetic fields. Journal of Geophysical Research: Space Physics, **126**(5): e2019JA027664.

Lindholm, F. 1939. Terrestrial Magnetism, Swedish Polar Year Expedition, Sveagruvan, Spitzbergen, 1932-1933, Swedish National Committee for Geodesy and Geophysics, Stockholm.

Liu, H., Lühr, H., Watanabe, S., Köhler, W., Henize, V., and Visser, P. 2006. Zonal winds in the equatorial upper thermosphere: decomposing the solar flux, geomagnetic activity, and seasonal dependencies. Journal of Geophysical Research: Space Physics, **111**(A7): 7307.

Lorentzen, D.A. 1999. Latitudinal and longitudinal dispersion of energetic auroral protons. Annales Geophysicae, **18**(1): 81–89.

Lorentzen, D.A., and Egeland, A. 2011. Dayside aurora—the fingerprint of the polar atmosphere. UNIS.

Lorentzen, D.A., and Moen, J. 2000. Auroral proton and electron signatures in the dayside aurora. Journal of Geophysical Research: Space Physics, **105**(A6): 12733–12745.

Lorentzen, D.A., Deehr, C.S., Minow, J.I., Smith, R.W., Stenbaek-Nielsen, H.C., Sigernes, F., et al. 1996. SCIFER-Dayside auroral signatures of magnetospheric energetic electrons. Geophysical Research Letters, **23**(14): 1885–1888.

Lorentzen, D.A., Kintner, P.M., Moen, J., Sigernes, F., Oksavik, K., Ogawa, Y., and Holmes, J. 2007. Pulsating dayside aurora in relation to ion upflow events during a northward interplanetary magnetic field (IMF) dominated by a strongly negative IMF BY. Journal of Geophysical Research: Space Physics, **112**(A3).

Lorentzen, D.A., Moen, J., Oksavik, K., Sigernes, F., Saito, Y., and Johnsen, M.G. 2010. In situ measurement of a newly created polar cap patch. Journal of Geophysical Research: Space Physics, **115**(A12): 12323.

Lorentzen, D.A., Shumilov, N., and Moen, J. 2004. Drifting airglow patches in relation to tail reconnection. Geophysical Research Letters, **31**(2).

Lorentzen, D.A., Sigernes, F., and Deehr, C.S. 1998. Modeling and observations of dayside auroral hydrogen emission Doppler profiles. Journal of Geophysical Research: Space Physics, **103**(A8): 17479–17488.

Lühr, H., Rother, M., Köhler, W., Ritter, P., and Grunwaldt, L. 2004. Thermospheric up-welling in the cusp region: evidence from CHAMP observations. Geophysical Research Letters,

Lund, E.J., Lessard, M.R., Sigernes, F., Lorentzen, D.A., Oksavik, K., Kintner, P.M., et al. 2012. Electron temperature in the cusp as measured with the scifer-2 sounding rocket. Journal of Geophysical Research: Space Physics, **117**(A6). doi:10.1029/2011JA017404.

Matzka, J., Stolle, C., Yamazaki, Y., Bronkalla, O., and Morschhauser, A. 2021. The geomagnetic kp index and derived indices of geomagnetic activity. Space weather : The International Journal of Research & Applications, **19**(5). doi:10.1029/2020SW002641.

Meriwether, J.W., Torr, D.G., Walker, J.C.G., and Nier, A.O. 1978. The O+(^{2}P) emission at 7320 Å in twilight. Journal of Geophysical Research: Space Physics, **83**(A7): 3311–3319.

Milan, S.E., Clausen, L.B.N., Coxon, J.C., Carter, J.A., Walach, M.T., Laundal, K., Østgaard, N., Tenfjord, P., Reistad, J., Snekvik, K., et al. 2017. Overview of solar wind–magnetosphere–ionosphere–atmosphere coupling and the generation of magnetospheric currents. Space Science Reviews, **206**: 547–573.

Moen, J., Lorentzen, D.A., and Sigernes, F. 1998. Dayside moving auroral forms and bursty proton auroral events in relation to particle boundaries observed by NOAA 12. Journal of Geophysical Research: Space Physics, **103**(A7): 14855–14863.

Moen, J., Oksavik, K., Abe, T., Lester, M., Saito, Y., Bekkeng, T.A., and Jacobsen, K.S. 2012. First in-situ measurements of hf radar echoing targets. Geophysical Research Letters, **39**(7). doi:10.1029/2012GL051407.

Moen, J., Oksavik, K., Alfonsi, L., Daabakk, Y., Romano, V., and Spogli, L. 2013. Space weather challenges of the polar cap ionosphere. Journal of Space Weather and Space Climate, **3**: A02. doi:10.1051/swsc/2013025.

Moser, C., LaBelle, J., Hatch, S., Moen, J.I., Spicher, A., Takahashi, T., et al. 2021. The cusp as a VLF Saucer Source: first rocket observations of long-duration VLF Saucers on the dayside.

Murphy, K.R., Rae, I.J., Halford, A.J., Engebretson, M., Russell, C.T., Matzka, J., et al. 2022. Gmag: an open-source python package for ground-based magnetometers. Frontiers in Astronomy and Space Sciences, **9**. doi:10.3389/fspas.2022.1005061.

Nishimura, Y., Lyons, L.R., Zou, Y., Oksavik, K., Moen, J.I., Clausen, L.B., et al. 2014. Day-night coupling by a localized flow channel visualized by polar cap patch propagation. Geophysical Research Letters, **41**(11): 3701–3709. doi:10.1002/2014GL060301.

Nishiyama, T., Kagitani, M., Furutachi, S., Iwasa, Y., Ogawa, Y., Tsuda, T.T., et al. 2024. The first simultaneous spectroscopic and monochromatic imaging observations of short-wavelength infrared aurora of N_2^+ meinel (0,0) band at 1.1 μm with incoherent scatter radar. Earth, Planets and Space, **76**:30. doi:10.1186/s40623-024-01969-x.

Nygrén, T., Aikio, A.T., Kuula, R., and Voiculescu, M. 2011. Electric fields and neutral winds from monostatic incoherent scatter measurements by means of stochastic inversion. Journal of Geophysical Research: Space Physics, **116**(A5): 5305.

Oksavik, K. 2020. The university of bergen global navigation satellite system data collection. DataverseNO.

Oksavik, K., Barth, V.L., Moen, J., and Lester, M. 2010. On the entry and transit of high-density plasma across the polar cap. Journal of Geophysical Research: Space Physics, **115**(A12).

Oksavik, K., Moen, J., and Carlson, H.C. 2004. High-resolution observations of the small-scale flow pattern associated with a poleward moving auroral form in the cusp. Geophysical Research Letters, **31**(11). doi:10.1029/2004GL019838.

Oksavik, K., Moen, J., Carlson, H.C., Greenwald, R.A., Milan, S.E., Lester, M., et al. 2005. Multi-instrument mapping of the small-scale flow dynamics related to a cusp auroral transient. Annales Geophysicae, **23**(7): 2657–2670. doi:10.5194/angeo-23-2657-2005.

Oksavik, K., Moen, J., Lester, M., Bekkeng, T.A., and Bekkeng, J.K. 2012. In situ measurements of plasma irregularity growth in the cusp ionosphere. Journal of Geophysical Research: Space Physics, **117**(A11).

Oksavik, K., van der Meeren, C., Lorentzen, D.A., Baddeley, L.J., and Moen, J. 2015. Scintillation and loss of signal lock from poleward moving auroral forms in the cusp ionosphere. Journal of Geophysical Research: Space Physics, **120**(10): 9161–9175. doi:10.1002/2015JA021528.

Partamies, N., Dol, B., Teissier, V., Juusola, L., Syrjäsuo, M., and Mulders, H. 2023. Auroral breakup detection in all-sky images by unsupervised learning. Annales Geophysicae Discussions.

Partamies, N., Tesema, F., and Bland, E. 2022a. Appearance and precipitation characteristics of high-latitude pulsating aurora. Frontiers in Astronomy and Space Sciences, **9**.

Partamies, N., Whiter, D., Kauristie, K., and Massetti, S. 2022b. Magnetic local time (MLT) dependence of auroral peak emission height and morphology. Annales Geophysicae, **40**(5): 605–618. doi:10.5194/angeo-40-605-2022.

Pilipenko, V.A., Kozyreva, O.V., Lorentzen, D.A., and Baddeley, L.J. 2018. The correspondence between dayside long-period geomagnetic pulsations and the open-closed field line boundary. Journal of Atmospheric and Solar-Terrestrial Physics, **170**: 64–74.

Prentice, E.F., Grøtte, M.E., Sigernes, F., and Johansen, T.A. 2021. Design of a hyperspectral imager using COTS optics for small satellite applications. *In* International Conference on Space Optics—ICSO 2020. *Edited by* Z. Sodnik, B. Cugny and N. Karafolas. SPIE. **11852**. p. 187. doi:10.1117/12.2599937.

Price, D.J., Whiter, D.K., Chadney, J.M., and Lanchester, B.S. 2019. High-resolution optical observations of neutral heating associated with the electrodynamics of an auroral Arc. Journal of Geophysical Research: Space Physics, **124**(11): 9577–9591. doi:10.1029/2019JA027345.

Pryse, S.E., Sims, R.W., Moen, J., Kersley, L., Lorentzen, D., and Denig, W.F. 2004. Evidence for solar-production as a source of polar-cap plasma. Annales Geophysicae, **22**(4): 1093–1102. doi:10.5194/angeo-22-1093-2004.

Reidy, J.A., Fear, R.C., Whiter, D.K., Lanchester, B., Kavanagh, A.J., Milan, S.E., et al. 2018. Interhemispheric survey of polar cap aurora. Journal of Geophysical Research: Space Physics, **123**(9): 7283–7306. doi:10.1029/2017JA025153.

Reidy, J.A., Fear, R.C., Whiter, D.K., Lanchester, B.S., Kavanagh, A.J., Price, D.J., et al. 2020. Multiscale observation of two polar cap arcs occurring on different magnetic field topologies. Journal of Geophysical Research: Space Physics, **125**(8): e2019JA027611. doi:10.1029/2019JA027611.

Roettger, J. 2000. Radar investigations of the mesosphere, stratosphere and the troposphere in svalbard. Advances in Polar Upper Atmosphere Research, **14**: 202–220.

Russell, C.T., Chappell, C.R., Montgomery, M.D., Neugebauer, M., and Scarf, F.L. 1971. Ogo 5 observations of the polar cusp on November 1, 1968. Journal of Geophysical Research, **76**(28): 6743–6764. doi:10.1029/JA076i028p06743.

Sakai, J., Hosokawa, K., Taguchi, S., and Ogawa, Y. 2014. Storm time enhancements of 630.0 nm airglow associated with polar cap patches. Journal of Geophysical Research: Space Physics, **119**(3): 2214–2228. doi:10.1002/2013JA019197.

Sarris, T.E., Talaat, E.R., Palmroth, M., Dandouras, I., Armandillo, E., Kervalishvili, G., et al. 2020. Daedalus: a low-flying spacecraft for in situ exploration of the lower thermosphere-ionosphere. Geoscientific Instrumentation, Methods and Data Systems, **9**(1): 153–191. doi:10.5194/gi-9-153-2020.

Semeter, J. 2003. Critical comparison of OII(732-733 nm), OI(630 nm), and N2(1PG) emissions in auroral rays. Geophysical Research Letters, **30**(5). doi:10.1029/2002GL015828.

Sigernes, F., Dyrland, M., Brekke, P., Chernouss, S., Lorentzen, D., Oksavik, K., and Deehr, C. 2011. Two methods to forecast auroral displays. Journal of Space Weather and Space Climate, **1**(1): A03. doi:10.1051/swsc/2011003.

Sigernes, F., Ellingsen, P.G., Partamies, N., Syrjäsuo, M., Brekke, P., Eriksen, H.S., et al. 2017. Video cascade accumulation of the total solar eclipse on svalbard 2015. Geoscientific Instrumentation, Methods and Data Systems, **6**(1): 9–14. doi:10.5194/gi-6-9-2017.

Sigernes, F., Fasel, G., Deehr, C.S., Smith, R.W., Lorentzen, D.A., Wetjen, L.T., et al. 1994a. Proton aurora on the dayside. Ge&Ae, **34**(5): 69–75.

Sigernes, F., Fasel, G., Minow, J., Deehr, C.S., Smith, R.W., Lorentzen, D.A., et al. 1996. Calculations and ground-based observations of pulsed proton events in the dayside aurora. Journal of Atmospheric and Terrestrial Physics, **58**(11): 1281–1291. doi:10.1016/0021-9169(95)00113-1.

Sigernes, F., Grøtte, M.E., Storvold, R., Syrjäsuo, M., Fortuna, J., and Johansen, T.A. 2018. Do it yourself hyperspectral imager for handheld to airborne operations. Optics Express, **26**(5). pp. 6021–6035. doi:10.1364/OE.26.006021.

Sigernes, F., Lloyd, N., Lorentzen, D.A., Neuber, R., Hoppe, U.P., Degenstein, D., et al. 2005. The red-sky enigma over Svalbard in December 2002. Annales Geophysicae, **23**(5): 1593–1602. doi:10.5194/angeo-23-1593-2005.

Sigernes, F., Lorentzen, D.A., Beehr, C.S., and Henriksen, K. 1994b. Calculation of auroral Bahner volume emission height profiles in the upper atmosphere. Journal of Atmospheric and Terrestrial Physics, **56**(4): 503–508. doi:10.1016/0021-9169(94)90199-6.

Sigernes, F., Lorentzen, D.A., Deehr, C.S., and Henriksen, K. 1993. Modulation of the auroral proton spectrum in the upper atmosphere. Journal of Atmospheric and Terrestrial Physics, **55**(9): 1289–1294. doi:10.1016/0021-9169(93)90053-2.

Sigernes, F., Lorentzen, D.A., Heia, K., and Svenøe, T. 2000. Multipurpose spectral imager. Applied Optics, **39**(18): 3143–3153. doi:10.1364/AO.39.003143.

Sigernes, F., Shumilov, N., Deehr, C.S., Nielsen, K.P., Svenøe, T., and Havnes, O. 2003. Hydroxyl rotational temperature record from the auroral station in Adventdalen, Svalbard (78°N, 15°E). Journal of Geophysical Research: Space Physics, **108**(A9). doi:10.1029/2001JA009023.

Southwood, D.J. 1987. The ionospheric signature of flux transfer events. Journal of Geophysical Research: Space Physics, **92**(A4): 3207–3213. doi:10.1029/JA092iA04p03207.

Spicher, A., Deshpande, K., Jin, Y., Oksavik, K., Zettergren, M., Clausen, L.B., et al. 2020. On the production of ionospheric irregularities via Kelvin–Helmholtz instability associated with cusp flow channels. Journal of Geophysical Research: Space Physics, **125**(6). doi:10.1029/2019JA027734.

Spicher, A., LaBelle, J., Bonnell, J.W., Roglans, R., Moser, C., Fuselier, S.A., et al. 2022. Interferometric study of ionospheric plasma irregularities in regions of phase scintillations and HF backscatter. Geophysical Research Letters, **49**(12): 1–11. doi:10.1029/2021GL097013.

Spicher, A., Miloch, W.J., Clausen, L.B., and Moen, J.I. 2015. Plasma turbulence and coherent structures in the polar cap observed by the ICI-2 sounding rocket. Journal of Geophysical Research: Space Physics, **120**(12): 959–10. doi:10.1002/2015JA021634.

Sutton, E.K., Nerem, R.S., and Forbes, J.M. 2012. Density and winds in the thermosphere deduced from accelerometer data. Journal of Space Crafts and Rockets, **44**(6): 1210–1219. doi:10.2514/1.28641.

Taguchi, S., Hosokawa, K., and Ogawa, Y. 2015a. Investigating the particle precipitation of a moving cusp aurora using simultaneous observations from the ground and space. Progress in Earth and Planetary Science, **2**(1): 1–11. doi:10.1186/s40645-015-0044-7.

Taguchi, S., Hosokawa, K., and Ogawa, Y. 2015b. Three-dimensional imaging of the plasma parameters of a moving cusp aurora. Journal of Atmospheric and Solar-Terrestrial Physics, **133**: 98–110. doi:10.1016/j.jastp.2015.08.012.

Taguchi, S., Hosokawa, K., Ogawa, Y., Aoki, T., and Taguchi, M. 2012. Double bursts inside a poleward-moving auroral form in the cusp. Journal of Geophysical Research: Space Physics, **117**(A12). doi:10.1029/2012JA018150.

Thomas, E.G., Hosokawa, K., Sakai, J., Baker, J.B., Ruohoniemi, J.M., Taguchi, S., et al. 2015. Multi-instrument, high-resolution imaging of polar cap patch transportation. Radio Science, **50**(9): 904–915. doi:10.1002/2015RS005672.

Van Der Meeren, C., Oksavik, K., Lorentzen, D., Moen, J.I., and Romano, V. 2014. GPS scintillation and irregularities at the front of an ionization tongue in the nightside polar ionosphere. Journal of Geophysical Research: Space Physics, **119**(10): 8624–8636. doi:10.1002/2014JA020114.

van der Meeren, C., Oksavik, K., Lorentzen, D.A., Paxton, L.J., and Clausen, L.B. 2016. Scintillation and irregularities from the nightside part of a Sun-aligned polar cap arc. Journal of Geophysical Research: Space Physics, **121**(6): 5723–5736. doi:10.1002/2016JA022708.

van der Meeren, C., Oksavik, K., Lorentzen, D.A., Rietveld, M.T., and Clausen, L.B. 2015. Severe and localized GNSS scintillation at the poleward edge of the nightside auroral oval during intense substorm aurora. Journal of Geophysical Research: Space Physics, **120**(12): 10607–10621. doi:10.1002/2015JA021819.

van Hazendonk, C.M., Baddeley, L., Laundal, K.M., and Chau, J.L. 2024. Detection and energy dissipation of ulf waves in the polar ionosphere: a case study using the eiscat radar. Journal of Geophysical Research: Space Physics, **129**(7): e2024JA032633.

Viljanen, A., and Häkkinen, L. 1997. Image magnetometer network. *In* Satellite-ground based coordination sourcebook. *Edited by* M. Lockwood, M.N. Wild and H.J. Opgenoorth. ESA Special Publication. **1198**. p. 111.

Von Savigny, C., McDade, I.C., Eichmann, K.U., and Burrows, J.P. 2012. On the dependence of the OH∗ Meinel emission altitude on vibrational level: SCIAMACHY observations and model simulations. Atmospheric Chemistry and Physics, **12**(18): 8813–8828. doi:10.5194/acp-12-8813-2012.

Whiter, D.K., Partamies, N., Gustavsson, B., and Kauristie, K. 2023. The altitude of green oi 557.7 nm and blue n_2^+ 427.8 nm aurora. Annales Geophysicae, **41**(1): 1–12. doi:10.5194/angeo-41-1-2023.

Whiter, D.K., Sundberg, H., Lanchester, B.S., Dreyer, J., Partamies, N., Ivchenko, N., et al. 2021. Fine-scale dynamics of fragmented aurora-like emissions. Annales Geophysicae, **39**(6): 975–989. doi:10.5194/angeo-39-975-2021.

Wright, A.N., Allan, W., and Damiano, P.A. 2003. Alfvén wave dissipation via electron energization. Geophysical Research Letters, **30**(16). doi:10.1029/2003GL017605.

Xiong, C., Lühr, H., Wang, H., and Johnsen, M.G. 2014. Determining the boundaries of the auroral oval from CHAMP field-aligned current signatures - Part 1. Annales Geophysicae, **32**(6): 609–622. doi:10.5194/angeo-32-609-2014.

Yagova, N., Nosikova, N., Baddeley, L., Kozyreva, O., Lorentzen, D.A., Pilipenko, V., and Johnsen, M.G. 2017. Non-triggered auroral substorms and long-period (1-4 mHz) geomagnetic and auroral luminosity pulsations in the polar cap. Annales Geophysicae, **35**: 365–376. doi:10.5194/angeo-35-365-2017.

Zhou, X.Y., Lummerzheim, D., Gladstone, R., and Gunapala, S. 2007. Feasibility of observing dayside aurora using NIR camera onboard high-altitude balloons. Geophysical Research Letters, **34**(3). doi:10.1029/2006GL028611.

Appendix A. Instrumentation

Table A1. Instrumentation at the Kjell Henriksen Observatory as of winter 2023–2024.

Instrument	Institution	Country
All-Sky Video Camera	University Centre in Svalbard (UNIS)	
BACC All-Sky Colour Camera	UNIS	Norway
Sony A7s All-Sky Camera	UNIS	Norway
All-Sky Airglow Camera	UNIS	Norway
Hyperspectral Tracker	UNIS	Norway
All-Sky Hyperspectral Camera	UNIS	Norway
Narrow field-of-view sCMOS tracker	UNIS	Norway
Meridian Imaging Svalbard Spectrometer	UNIS	Norway
Polar Research Ionospheric Doppler Experiment	UNIS	Norway
2 × Tracker Cameras	UNIS	Norway
Automatic Weather Station	UNIS	Norway
Meridian Scanning Photometer	UNIS	Norway/USA
1/2 m Green Ebert–Fastie Spectrometer	UNIS	Norway/USA
1m Silver Ebert–Fastie Spectrometer	UNIS	Norway/USA
All-Sky Imager	University of Oslo	Norway
Scintillation and TEC Receiver	University of Bergen	Norway
Fluxgate Magnetometer	University of Tromsø (UiT)	Norway
1/2 m White Ebert–Fastie Spectrometer	UiT/UNIS	Norway
All-Sky Colour Imager	University College London (UCL)	UK
Imaging Fabry–Perot Interferometer	UCL	UK
Scanning Doppler Imager	UCL	UK
Spectrographic Imaging Facilities	University of Southampton	UK
Auroral Spectrograph	National Institute of Polar Research (NIPR)	Japan
NIR Spectrograph	NIPR	Japan
NIR Camera	NIPR	Japan
All-Sky Airglow Imager	Kyoto University	Japan
Auroral Radio Spectrograph	Tohoku University	Japan
GNSS Receivers	Nagoya University	Japan
Monochromatic Auroral Imager	Polar Research Institute of China (PRIC)	China
Single-wave Auroral Imager	PRIC	China
Fabry–Perot Interferometer	PRIC	China
Fluxgate Magnetometer	PRIC	China
Induction Magnetometer	PRIC	China
Aurora All-Sky Camera	Korean Polar Research Institute (KOPRI)	Korea
Fabry–Perot Interferometer	KOPRI	Korea
The Hot Oxygen Doppler imager	New Jersey Institute of Technology	USA
2-axis Search-coil magnetometer	University of New Hampshire	USA
UCB-GNSS receiver	University of Colorado, Boulder	USA
HF acquisition system	Institute of Radio Astronomy	Ukraine
UHF Ground station	National Institute of Aeronautics	Indonesia
UHF Ground station	Technische Universität Berlin	Germany